Check for updates

Received: 13 September 2022 | Revised: 18 January 2023 | Accepted: 23 January 2023

DOI: 10.1002/cne.25462

RESEARCH ARTICLE

JCN RESEARCH IN SYSTEMS NEUROSCIENCE THE JOURNAL OF COMPARATIVE NEUROLOGY WILEY

Neuronal circuits within the homing pigeon hippocampal formation

Noemi Rook[1] | Martin Stacho[1] | Ariane Schwarz[1] | Verner P. Bingman[2,3] | Onur Güntürkün[1]

[1]Department of Biopsychology, Institute of Cognitive Neuroscience, Faculty of Psychology, Ruhr-University Bochum, Bochum, Germany

[2]Department of Psychology, Bowling Green State University, Bowling Green, Ohio, USA

[3]J.P. Scott Center for Neuroscience, Mind and Behavior, Bowling Green State University, Bowling Green, Ohio, USA

Correspondence
Noemi Rook, Department of Biopsychology, Institute of Cognitive Neuroscience, Faculty of Psychology, Ruhr-University Bochum, Universitätsstraße 150, D-44780 Bochum, Germany.
Email: Noemi.rook@rub.de

Funding information
Alexander Humboldt Foundation; European Research Council, Grant/Award Numbers: ERC-2020-ADG, LS5, GA No. 101021354; Deutsche Forschungsgemeinschaft (DFG), Grant/Award Numbers: 395940726(Neu06), 316803389(A01)

Abstract

The current study aimed to reveal in detail patterns of intrahippocampal connectivity in homing pigeons (*Columba livia*). In light of recent physiological evidence suggesting differences between dorsomedial and ventrolateral hippocampal regions and a hitherto unknown laminar organization along the transverse axis, we also aimed to gain a higher-resolution understanding of the proposed pathway segregation. Both in vivo and high-resolution in vitro tracing techniques were employed and revealed a complex connectivity pattern along the subdivisions of the avian hippocampus. We uncovered connectivity pathways along the transverse axis that started in the dorsolateral hippocampus and continued to the dorsomedial subdivision, from where information was relayed to the triangular region either directly or indirectly via the V-shaped layers. The often-reciprocal connectivity along these subdivisions displayed an intriguing topographical arrangement such that two parallel pathways could be discerned along the ventrolateral (deep) and dorsomedial (superficial) aspects of the avian hippocampus. The segregation along the transverse axis was further supported by expression patterns of the glial fibrillary acidic protein and calbindin. Moreover, we found strong expression of Ca^{2+}/calmodulin-dependent kinase IIα and doublecortin in the lateral but not medial V-shape layer, indicating a difference between the two V-shaped layers. Overall, our findings provide an unprecedented, detailed description of avian intrahippocampal pathway connectivity, and confirm the recently proposed segregation of the avian hippocampus along the transverse axis. We also provide further support for the hypothesized homology of the lateral V-shape layer and the dorsomedial hippocampus with the dentate gyrus and Ammon's horn of mammals, respectively.

KEYWORDS
avian hippocampus, calbindin, CaMKIIα, doublecortin, GFAP, intrahippocampal circuitry, topography, tracing

Noemi Rook and Martin Stacho contributed equally to this work.

This is an open access article under the terms of the Creative Commons Attribution License, which permits use, distribution and reproduction in any medium, provided the original work is properly cited.
© 2023 The Authors. *The Journal of Comparative Neurology* published by Wiley Periodicals LLC.

1 | INTRODUCTION

Many bird species have outstanding spatial abilities as visible during migration, homing, or food caching (Clayton & Dickinson, 1998; Mouritsen et al., 2016). These skills rely heavily on the integrity of the hippocampus (HC) as damage to this structure is associated with an impairment in numerous spatial functions (Gagliardo et al., 1999, 2014; Pravosudov et al., 2006; Sherry & Vaccarino, 1989). In addition, it has been found that caching bird species have a larger HC compared with those that do not cache (Garamszegi & Eens, 2004; Garamszegi & Lucas, 2005; Lucas et al., 2004). Although the anatomy and physiology of the avian HC have been investigated in several studies (e.g., Atoji & Wild, 2004; Atoji et al., 2016; Ben-Yishay et al., 2021; Erichsen et al., 1991; Herold et al., 2014; Kahn et al., 2003; Payne et al., 2021; Siegel et al., 2002; Szkely & Krebs, 1996), much is still unknown about the intrahippocampal neuronal networks that support these spatial abilities. Neurons in the homing pigeon HC display robust spatial response properties (Hough & Bingman, 2004; Siegel et al., 2005, 2006; Kahn et al., 2008), which interestingly do not completely align with so-called place cells in rats. More recent studies, however, indicate that the avian HC does contain place cells, at least in food-caching titmice and nonhoarding zebra finches (Payne et al., 2021), as well as head direction cells (Apostel & Rose, 2021; Ben-Yishay et al., 2021) and sharp wave ripples (SWRs) (Payne et al., 2021), and thus physiological properties that are hallmarks of hippocampal function in mammals (Hartley et al., 2014; Moser et al., 2008). Moreover, the existence of theta oscillations was reported for awake pigeons (Siegel et al., 2000), but could, however, not be replicated in subsequent studies investigating sleeping pigeons and other avian species (Martinez-Gonzalez et al., 2008; Payne et al., 2021).

Similar to the avian HC, the mammalian HC is also strongly involved in spatial tasks such as navigation and the retention of spatial information (Broadbent et al., 2004; Geva-Sagiv et al., 2015; Morandi-Raikova & Mayer, 2022). However, despite these striking functional and physiological similarities, the avian and mammalian HC show vastly different cytoarchitectures. While the mammalian HC is a three-layered cortex, consisting of a molecular, a cellular, and a polymorphic layer, this clear anatomical organization is not present in birds (Amaral & Witter, 1989; Striedter, 2016). The HC is a phylogenetically old structure that probably was already present in the last common ancestor of birds and mammals. Thus, the difference in anatomical organization at the macroscopic level could be the result of the more than 300 million years of independent evolution (Striedter, 2016). In light of the functional and physiological similarities of the avian and mammalian HC, the question arises whether some network connectivity or cellular features may be evolutionarily conserved, despite the profound macroscopic differences.

In mammals, the HC is typically subdivided along the transverse axis into the dentate gyrus (DG), the CA fields of the cornu ammonis (Ammon's horn), and the subiculum. Both the Ammon's horn and the DG show a three-layered organization where a cellular layer is flanked between two plexiform layers, which in turn have different sublayers (Nieuwenhuys et al., 2007). The Ammon's horn is typically subdivided into the areas CA1, CA2, CA3, and CA4 that can be differentiated by the density and size of pyramidal neurons in the cellular layer. The subiculum is the area where the three-layered HC transitions into the six-layered entorhinal cortex (EC) in the parahippocampal region. The EC can be distinguished from other neocortical structures as it exhibits a fiber layer with low cell numbers (lamina dissecans) instead of the typical layer 4 (Canto et al., 2008). The EC is also the main input structure into the HC and forms a link between the HC and the remaining neocortex (Kerr et al., 2007). Within the HC, the main information flow follows the trisynaptic pathway, in which the DG receives input from the EC through the perforant path (synapse 1), from where information is forwarded to the CA3 area via mossy fibers (synapse 2). Finally, CA3 provides input to CA1 via the Schaffer collaterals (synapse 3) (Amaral & Witter, 1995).

In a similar manner, the avian HC can be subdivided into subregions along the transverse axis based on connectivity as well as cyto- and chemoarchitecture (Atoji & Wild, 2004, 2006; Atoji et al., 2016; Casini et al., 1986; Erichsen et al., 1991; Herold et al., 2014; Kahn et al., 2003). To date, various studies have proposed different subdivisions, but most agree that the avian hippocampal formation (HF) can be subdivided into a dorsolateral (DL), a dorsomedial (DM), and a ventral V-shaped area (Figure 1) (Atoji & Wild, 2006; Atoji et al., 2016; Erichsen et al., 1991; Gupta et al., 2012; Herold et al., 2014; Kahn et al., 2003; Siegel et al., 2002). DL can be distinguished from the laterally adjacent area corticoidea dorsolateralis (CDL) based on decreasing thickness and from the medially adjacent DM based on a sulcus on the ventricular side of the HF, which extends along the anterior posterior axis of the HF (Atoji & Wild, 2004). DL can be furthermore subdivided into a dorsal and ventral component based on connectivity and receptor architecture (Atoji & Wild, 2004; Herold et al., 2014). For DM, different subdivisions have been proposed. While DM has been subdivided into a dorsal (DMd) and ventral (DMv) component based on hippocampal receptor densities (Herold et al., 2014), other studies further distinguished three small regions within the dorsal DM based on cell morphology and cytoarchitecture (Atoji & Wild, 2004). Moreover, the V-shaped area consists of a triangular region (Tr) that is surrounded by a thin V-shaped layer that is clearly visible due to its higher neuron density (Atoji & Wild, 2004; Erichsen et al., 1991; Krebs et al., 1991). This V-shaped layer can be further subdivided into a lateral (Vl) and a medial (Vm) component that both are coated by cell poor fiber layers. These fiber layers have been referred to as the paraventricular (pfz) and medial fiber zone (mfz), respectively (Atoji & Wild, 2004, 2006). It needs to be noted that these V-shaped layers differ between birds and are not clearly seen, for example, in chickens, ostriches, and parrots (Striedter, 2016). So far, the consensus is that DL, DM, and the V-shaped area are reciprocally connected with each other. The main extrahippocampal inputs seem to arrive from the hyperpallium, CDL, and the thalamus, providing the avian HF with sensory information (Atoji & Wild, 2004, 2005; Casini et al., 1986). Moreover, the main extrahippocampal output of the HF is sent to the

10969861, 2023, 7, Downloaded from https://onlinelibrary.wiley.com/doi/10.1002/cne.25462 by Cochrane Germany, Wiley Online Library on [28/04/2023]. See the Terms and Conditions (https://onlinelibrary.wiley.com/terms-and-conditions) on Wiley Online Library for rules of use; OA articles are governed by the applicable Creative Commons License

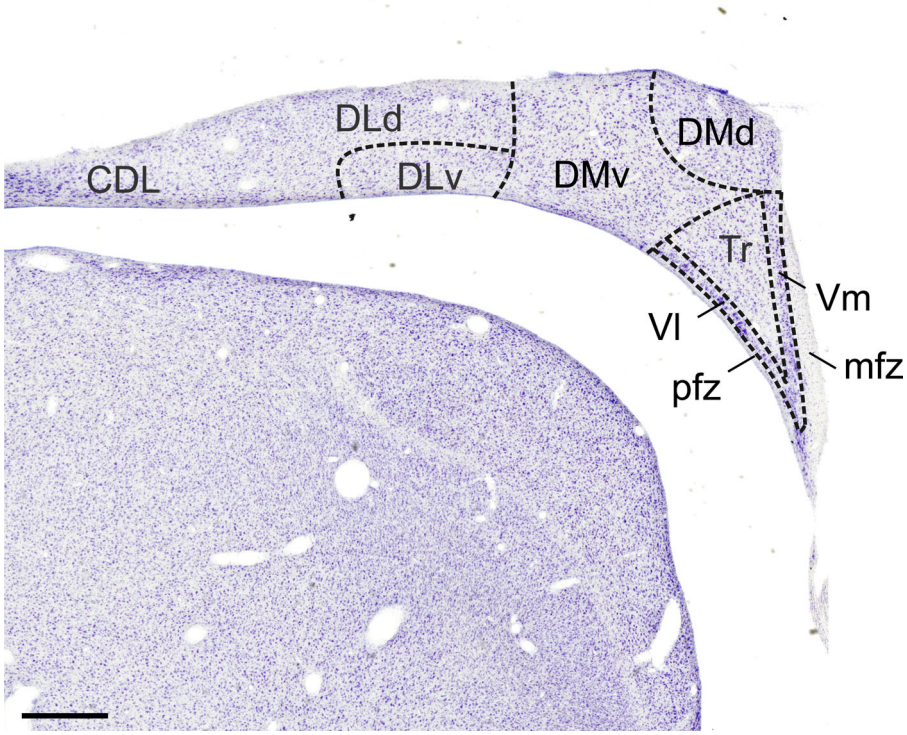

FIGURE 1 Nissl-stained section indicating the subdivisional organization of the homing pigeon hippocampal formation (HF). Nissl-stained coronal section of the HF showing subdivisional boundaries according to Herold et al. (2014). The HF of pigeons can be subdivided into seven regions: the V-complex, which contains a lateral (Vl) and medial (Vm) cell layer, and an inner triangular area (Tr). The V-shaped cell layers are flanked by two fiber zones (pfz and mfz). Moreover, the dorsomedial region can be subdivided into ventral (DMv) and dorsal (DMd) subdivisions. Likewise, the dorsolateral region contains a ventral (DLv) and dorsal (DLd) component. Scale bar represents 500 μm.

septum and the lateral hypothalamus (Atoji & Wild, 2004; Casini et al., 1986).

Although several studies have already investigated the intrinsic and extrahippocampal connectivity of the three major subdivisions (Atoji & Wild, 2004; Hough et al., 2002; Kahn et al., 2003), many open questions remain. Up to now, the local connectivity pattern of the avian HF was only studied using in vivo tracer injections. Given the small size of the HF and its complex three-dimensional structure, it is extremely difficult to obtain a comprehensive description of the projections between the HF subcomponents. We therefore employed both in vitro and in vivo tracing procedures to obtain a more complete understanding of the intrahippocampal connections of the pigeon hippocampal complex. These techniques are complementary as in vivo tracing is better suited to study long-range connectivity, while in vitro tracing offers greater spatial resolution for focal injections into small subareas. Moreover, we investigated the connectivity along the transverse axis focusing especially on a possible anatomical segregation between dorsomedial (superficial) and ventrolateral (deep) HF, which has recently been suggested based on physiological (Payne et al., 2021) and neurochemical (Medina et al., 2017; Redies et al., 2001) evidence. As this has not been identified in previous tracing experiments, our study aimed to gain a higher resolution understanding of HF intrinsic connectivity with respect to the potential segregation of subdivisions along the transverse axis.

2 | METHODS

2.1 | Animals

This study included a total of 38 homing pigeons (*Columba livia*), from which 20 were used for in vivo tracings and 18 further pigeons for in vitro tracings. All animals were obtained from local breeders and were individually housed in wire-mesh cages. Housing rooms were controlled for temperature, humidity, and day/night cycles (12-h light–dark cycle). All experiments were performed according to the guidelines regarding the care and use of animals adopted by the German Animal Welfare Law for the prevention of cruelty to animals in agreement with the Directive 2010/63/EU of the European Parliament and of the Council of 22 September 2010, and were approved by the animal ethics committee of the Landesamt für Natur, Umwelt und Verbraucherschutz NRW, Germany. All efforts were made to minimize the number of animals used and to minimize their suffering.

2.2 | Surgical procedure and in vivo tracer injection

In vivo tracing experiments required a surgical procedure for tracer injection. Therefore, the pigeons were anesthetized using a mixture of ketamine (Ketavet 100 mg/mL, Zoetis GmbH, 52.5 mg per kg body

10969861, 2023, 7, Downloaded from https://onlinelibrary.wiley.com/doi/10.1002/cne.25462 by Cochrane Germany, Wiley Online Library on [28/04/2023]. See the Terms and Conditions (https://onlinelibrary.wiley.com/terms-and-conditions) on Wiley Online Library for rules of use; OA articles are governed by the applicable Creative Commons License

weight) and xylazine (Rompun 20 mg/mL, Bayer Vital GmbH, 4.5 mg per kg body weight) together with isoflurane (1.5–2.5% in pure oxygen, Forane 100%, Abbott GmbH & Co. KG, Wiesbaden, Germany). Once the depth of anesthesia was sufficient, the birds were placed in a stereotactic apparatus and their heads were fixed. Feathers were removed from the scalp and an incision was made to expose the skull. Craniotomies above the injection targets were performed to gain access to the brain. After the meninges were opened, a glass micropipette with an inner diameter of 15–20 μm filled with Choleratoxin subunit B (CTB, Sigma, Germany) was lowered into the brain to the intended injection targets. CTB is a tracer with strong retrograde and weak anterograde transport (Köbbert et al., 2000). Stereotactic coordinates were determined using the stereotactic atlas of the pigeon brain (Karten & Hodos, 1967). A volume of 200–400 nL of tracer was pressure injected using a Nanoliterinjector 2000 (WPI, Sarasota, USA). Injections were only performed in one hemisphere per animal. After 2 days, the pigeons were perfused.

2.3 | In vitro tracing

For the in vitro tracings, the pigeons were anesthetized with equithesin (0.45 mL/100 g body weight) and subsequently decapitated. After a rapid dissection of the brains, they were placed in ice-cooled sucrose-substituted Krebs solution (210 mM sucrose, 3 mM KCl, 3 mM $MgCl_2 \cdot 6H_2O_2$, 23 mM $NaHCO_3$, 1.2 mM $NaH_2PO_4 \cdot H_2O$, 11 mM β-D-glucose) for 2 min. After that, brains were cut with a vibratome (VT1000S, Leica, Germany) into coronal slices of 800 μm thickness. The slices then remained at room temperature in artificial cerebrospinal fluid (ACSF; 120 mM NaCl, 3 mM KCl, 1 mM $MgCl_2 \cdot 6H_2O_2$, 23 mM $NaHCO_3$, 1.2 mM $NaH_2PO_4 \cdot H_2O$, 2 mM $CaCl_2 \cdot 2H_2O$, 11 mM β-D-glucose), which was constantly flooded with carbogen (95% O_2, 5% CO_2). For the injections, slices were moved to a separate chamber and biocytin crystals (Santa Cruz Biotechnology, USA) were placed on the different hippocampal subdivisions with a glass micropipette. Biocytin has strong anterograde and weaker retrograde transport (Köbbert et al., 2000). The sections were replaced in the carbogenized ACSF, where they remained for 4–6 h before being immersion fixated for 12 h using 4% paraformaldehyde in 0.12 M PB (pH 7.4). After fixation, the slices were transferred to a 30% sucrose solution (in PBS, pH 7.4) for cryoprotection. Once the sections had sunk, they were further sectioned into 35-μm-thick slices on a freezing microtome (Leica, Germany).

2.4 | Perfusion and brain sectioning

The animals of the in vivo tracing experiment were anesthetized using equithesin (0.45 mL/100 g body weight) prior to the perfusion. They were then transcardially perfused with 0.9% NaCl, after which 4°C cold paraformaldehyde (4% in 0.12 M PB, pH 7.4) was applied for tissue fixation. After sufficient fixation, the brains were extracted from the skull and further fixated in a postfix solution (4% paraformaldehyde and 30% sucrose in 0.12 M PB) at 4°C for 2 h. Afterwards, brains were transferred to a sucrose solution for cryoprotection (30% sucrose in PBS, pH 7.4) until sinking to the bottom. Subsequently, they were embedded in gelatin (15% gelatin and 30% sucrose in PBS), which was again fixated in postfix solution for 24 h. Using a freezing microtome (Leica, Germany), the brains were sectioned coronally with 30–40 μm thickness before further staining procedures were performed on every fifth slice.

2.5 | 3,3′-Diaminobenzidine staining

To visualize biocytin, CTB, and doublecortin (DCX) signals, a 3,3′-diaminobenzidine (DAB) staining procedure was used with nickel and cobalt intensification. First, the slices were rinsed for 10 min in PBS and incubated for 30 min in 0.3% hydrogen peroxide (H_2O_2) in distilled water to block endogenous peroxidases. After that, slices were rinsed for 3 × 10 min in PBS. For CTB and DCX stainings, slices were transferred to 10% normal horse or rabbit serum in PBST (PBS with 0.3% Triton-X-100) for 1 h to inhibit nonspecific binding. Following this step, the CTB and DCX slices were incubated with either a polyclonal goat anti-CTB antibody (1:10 000 in PBST; Millipore) or a goat anti-DCX antibody (1:1000 in PBST, sc8066 Santa Cruz) at 4°C overnight, after which the sections were rinsed in PBS (3 × 10 min). For the next step, the slices were incubated for 60 min at room temperature in a secondary biotinylated rabbit anti-goat antibody (1:200 in PBST; Vector Laboratories—Vectastain Elite ABC kit). After further rinsing in PBS (3 × 10 min), all slices (i.e., CTB, DCX, and biocytin sections) were then incubated in an avidin–biotin-peroxidase complex solution (Vector Laboratories—Vectastain Elite ABC kit; 1:100 in PBST) at room temperature for 1 h (serum, primary, and secondary antibody steps were not necessary for the biocytin slices). The slices received further rinsing in PBS (3 × 10 min), after which they were rinsed for 5 min in 0.1 M sodium acetate buffer (pH 6.0). Following this rinsing step, the sections were moved to the DAB solution consisting of DAB (0.2 mg/mL), ammonium nickel sulfate (25 mg/mL), cobalt chloride (0.4 mg/mL), ammonium chloride (0.4 mg/mL), and β-D-glucose (4 mg/mL) in 0.1 M sodium acetate buffer (pH 6.0). The staining reaction was started by the addition of glucose oxidase (80—100 μL in 50 mL DAB solution) that oxidates the β-D-glucose that was included in the DAB solution. The reaction lasted 30 min (staining intensity was visually controlled), and the reaction solution was changed every 10 min. Rinsing the slices in 0.1 M sodium acetate buffer (pH 6.0; 3 × 5 min) stopped the reaction. After the DAB reaction and additional rinsing (3 × 10 min in PBS), the sections were mounted on glass slides covered in gelatin, dehydrated in ethanol and xylene, and cover-slipped using DPX (Fluka, Munich, Germany). Some of the biocytin sections were also counterstained with Nissl.

2.6 | Fluorescence staining

For the characterization of the neurochemical profile of the pigeon HF, immunohistochemical fluorescence stainings were performed against

10969861, 2023, 7, Downloaded from https://onlinelibrary.wiley.com/doi/10.1002/cne.25462 by Cochrane Germany, Wiley Online Library on [28/04/2023]. See the Terms and Conditions (https://onlinelibrary.wiley.com/terms-and-conditions) on Wiley Online Library for rules of use; OA articles are governed by the applicable Creative Commons License

four markers in six animals each. The markers Ca^{2+}/calmodulin-dependent kinase IIα (CaMKIIα), calbindin, and glial fibrillary acidic protein (GFAP) were visualized in this study using the respective antibodies rabbit anti-CaMKIIα antibody (abcam [ab5683], Cambridge, US), rabbit anti-calbindin antibody (CB-38a, Swant, CH), and rat anti-GFAP antibody (AB_2532994, Invitrogen, Darmstadt, Germany). Primary antibody specificity was ensured by comparing the resulting staining patterns of our study with previous reports in pigeons using the same DCX (sc8066, Santa Cruz) and calbindin (CB-38a, Swant) antibodies (Mehlhorn et al., 2022), as well as GFAP antibody (AB_2532994, Invitrogen) (Rook et al., 2021). All fluorescence stainings were performed as follows: brain sections were first washed in PBS (3 × 10 min), after which they were incubated in 10% normal horse serum in PBST for half an hour. Following that, the slices were transferred to the primary antibody solution (1:1000 in PBST), where they stayed for 72 h at 4°C. Next, they were rinsed again (3 × 10 min in PBS) before being incubated in the secondary antibody for 1 h (1:500 in PBST goat anti-rat Alexa Fluor 488, goat anti-rabbit Alexa Fluor 594 [Invitrogen]). After further rinsing (3 × 10 min in PBS), slices were mounted on glass slides (Superfrost® Plus, Thermo Scientific).

2.7 | Microscopy and analysis

The slices were analyzed with a ZEISS Imager.M1 AXIO microscope equipped with an AxioCam MRm ZEISS 60N-C 2/3″ 0.63× camera. The ZEISS filter settings of 45 (excitation: BP 560/40; beam splitter: FT 585; emission: BP 630/75) and 38 (excitation: BP 470/40; beam splitter: FT 495; emission: BP 525/50) were used for the analysis of the fluorescence staining. Pictures of the relevant slices were taken via the computer software AxioVision (AxioVision, Version: 4.8.1.0, Zeiss, Germany). Color, contrast, and brightness adjustments were accomplished via the Zen 3.5 lite (Zeiss, Germany) software as well as CorelDRAW X5 (Version 15.2.0.686; Corel Corporation). The cell size measurements for the calbindin staining were performed in Zen 3.5 lite (Zeiss, Germany) with help of the spline tool.

3 | RESULTS

3.1 | In vivo tracing experiments in the HF

We first performed in vivo tracings to investigate longer distance connectivity within the HF. For our in vivo injections and the analysis of the data, we relied on the hippocampal subdivisional scheme described in Herold et al. (2014) (Figure 1). Tracer injections could be clustered into three main groups (Figure 2). The first group included cases where the tracer was confined to DMv (Figure 2 [red]). The second group consisted of cases where tracer spread was found in DMd, Tr, and occasionally in the most medial part of DMv (Figure 2 [green]). The injections of the third group were mostly restricted to the V-shaped area (Figure 2 [blue]).

Injections that were confined to DMv resulted mainly in retrogradely labeled cells in Vl, DMd, DLv, and to a lesser extent in Tr (Figure 2 [red]). Moreover, anterogradely labeled fibers could mainly be observed in Tr and DLd (Figure 2; e.g., case 115). In contrast, tracer injections targeting mainly DMd and Tr led to anterogradely labeled fibers in DMv and Vm and retrograde labeling in DLd, DLv, CDL, and to a lesser extent in Vm (Figure 2 [green]). Similarly, injections into the V-shaped region resulted in retrograde labeling in DLd, DLv, CDL, DMd, and DMv (Figure 2 [blue]).

Comparing the pattern of retrograde labeling revealed different projection patterns of the three injection groups. Injections that were confined to DMv resulted in extensive labeling in Vl and DMd (Figures 2 [red] and 3a). In contrast, retrograde labeling in Vl was absent after tracer injections targeting mainly DMd and Tr (Figures 2 [green] and 3b). Rather, injection cases of this group led to a sparse labeling of neurons within Vm (Figure 2 [green]). Thus, the in vivo tracing data indicate that Vl and Vm project to different hippocampal subdivisions. While Vl mainly innervates DMv, Vm primarily projects to DMd and Tr. The projection to DMd is probably also reciprocal as retrogradely labeled cells could be found within DMd following injections into the V-shaped area (Figures 2 and 3c,f).

The three injection groups also revealed different projection targets of DLd and DLv. For example, injections into DMv resulted in retrograde labeling in DLv, but not in DLd (Figures 2 [red] and 3a,g). In contrast, injections into DMd led to retrogradely labeled neurons in both DLd and DLv (Figures 2 [green] and 3b,h). Similarly, retrograde labeling could be seen in both DL subdivisions after injections targeting the V-shaped area (Figures 2 [blue] and 3c,i). Finally, we analyzed retrograde labeling within the CDL for all three injection groups. While labeling in CDL was nearly absent after DMv injections (Figures 2 [red] and 3a,j), many retrogradely labeled neurons could be observed after DMd and Tr injections (Figures 2 [green] and 3b,k). Injections into the V-shaped area resulted in the strongest labeling in CDL, indicating that this subregion is the main target of CDL projections (Figures 2 [blue] and 3c,l). In general, labeling in CDL was mainly found in its central part (Figure 2).

We noticed that the DMv group differed in their afferents and efferent targets depending on whether the injections were rather located in either the dorsal (DMvd) or ventral (DMvv) parts of DMv. For example, DMvd but not DMvv injections labeled neurons within DMd (Figure 4a,b,d,e). Furthermore, retrograde labeling in Vl was stronger for injections targeting DMvv compared to injections targeting DMvd (Figure 2; case 418 vs. 417). Likewise, tracer injections that were confined to DMvv labeled descending fibers running across the lateral half of Tr, whereas DMvd injections resulted in descending fibers within the medial half of Tr (Figure 4a,c,d,f). Last but not least, injections focused on DMd and Vm labeled neurons exclusively in DMvd, but not DMvv (Figure 4g,h). In CTB injections covering both DMvv and DMvd, we observed that fibers leaving DMvd targeted DLd (few of them crossed toward DLv), while there were fewer fibers that left the DMvv and reached the DLv (Figure 3a,g).

10969861, 2023, 7, Downloaded from https://onlinelibrary.wiley.com/doi/10.1002/cne.25462 by Cochrane Germany, Wiley Online Library on [28/04/2023]. See the Terms and Conditions (https://onlinelibrary.wiley.com/terms-and-conditions) on Wiley Online Library for rules of use; OA articles are governed by the applicable Creative Commons License

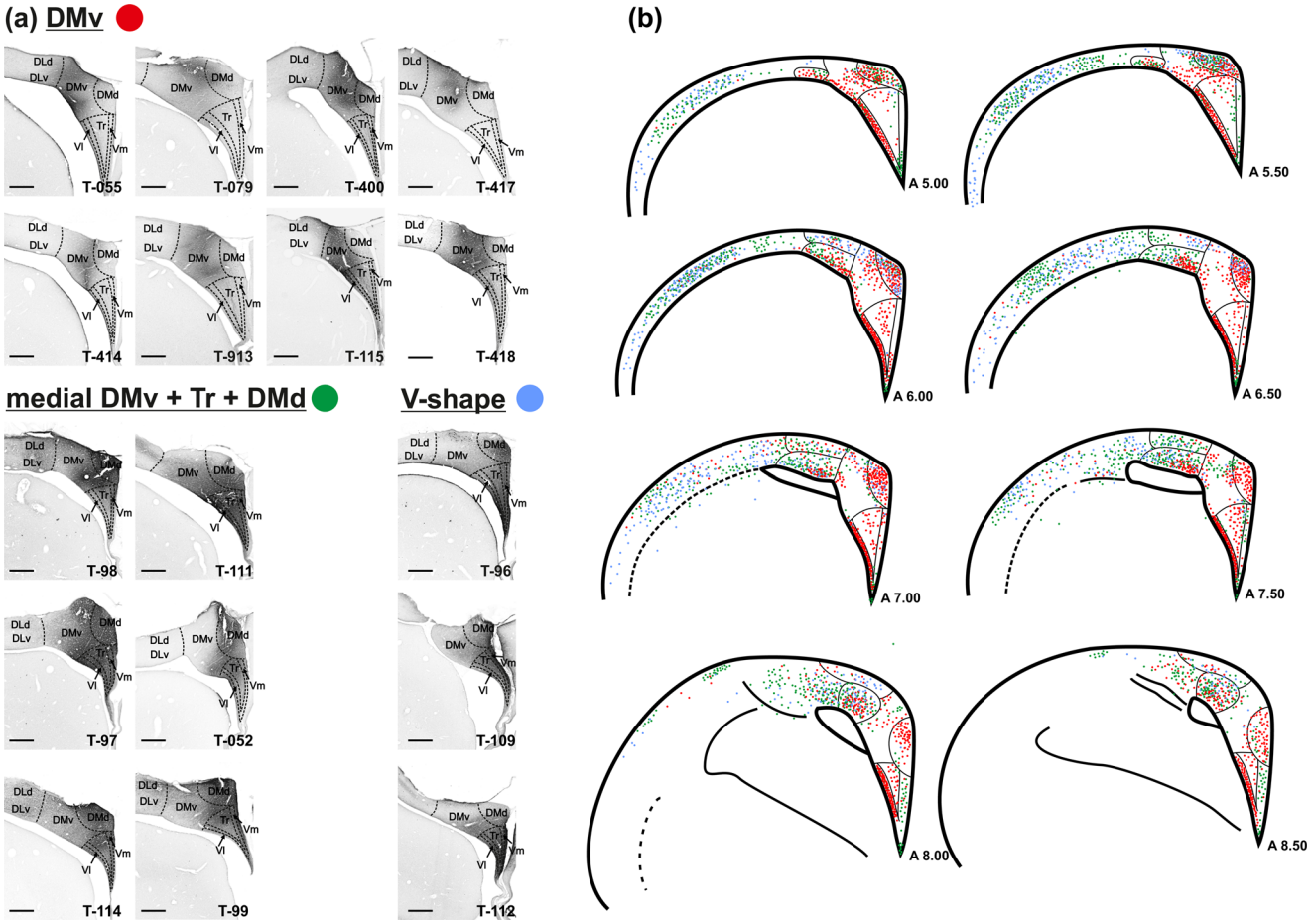

FIGURE 2 Retrograde labeling in the hippocampal formation (HF) and area corticoidea dorsolateralis (CDL) following injections into different subareas. The in vivo injections into the HF were separated into three groups based on their target areas. (a) Group 1 (red) consisted of cases where injections were restricted to DMv. Group 2 (green) included cases with injections into DMd, Tr, and medial DMv. Group 3 (blue) consisted of cases where injections were focused on the V-shaped area. (b) Summary of retrograde labeling at different rostrocaudal planes (A5.0–A8.5) for the different injection groups. Red dots represent labeled neurons for group 1, green dots represent labeled neurons for group 2, and blue dots represent labeled neurons for group 3. Scale bars represent 500 μm.

Besides that, we saw long-range fibers leaving from both DMvd and DMvv and running along the dorsal and ventral aspect of the CDL, respectively.

3.2 | Neurochemical profile of the avian HF

To better characterize and delineate the boundaries of hippocampal subdivisions, especially with respect to the observed differences in the projection patterns of DMvd and DMvv, we stained hippocampal sections against different immunohistochemical markers such as calbindin, DCX, CaMKIIα, and GFAP. Calbindin-expressing cells were scattered among all hippocampal subdivisions including DMvd, DMd, and DMvv (Figure 5). The density and size of calbindin-positive neurons within DMvd and DMd appeared somewhat larger compared to those in DMvv (Figure 5). The labeled cells in DMvd had an area of approximately 135 μm^2 ± 6 *SEM* (Figure 5b,f,j,n), and in DMd 165 μm^2 ± 10 *SEM* (Figure 5d,h,l,p). By contrast, the cells in DMvv had an area of approximately 83 μm^2 ± 6 *SEM* (Figure 5c,g,k,o), indicating a 2-fold difference in size. These differences provide further justification for the segregation of DMv into a dorsal and a ventral part.

Furthermore, we took a closer look at GFAP expression, which is a marker for astrocytes and radial glia within the brain. The GFAP staining labeled a thin cell layer along the pial surface of the HF as well as cells located in the periventricular area of DMvv and DL characterized by dense radial processes (Figure 6). Furthermore, a band of astrocytes was usually observed reaching from DMv to Tr (Figure 6a,e,i,m). This band of cells, however, did not clearly dissociate between DMvv and DMvd but was distributed rather centrally, occurring in both subdivisions. Nevertheless, as indicated above, the DMvv (and the lateral V-shaped layer) displayed high density of GFAP-positive fibers indicating radial glia in these areas (Figure 6c,g,k,o). By contrast, the density of GFAP-positive fibers seemed lower in DMvd (Figure 6b,f,j,n) and DMd (Figure 6d,h,l,p). Thus, the GFAP staining might support the segregation of DMv into dorsal and ventral subregions, but also adds another level of complexity.

10969861, 2023, 7, Downloaded from https://onlinelibrary.wiley.com/doi/10.1002/cne.25462 by Cochrane Germany, Wiley Online Library on [28/04/2023]. See the Terms and Conditions (https://onlinelibrary.wiley.com/terms-and-conditions) on Wiley Online Library for rules of use; OA articles are governed by the applicable Creative Commons License

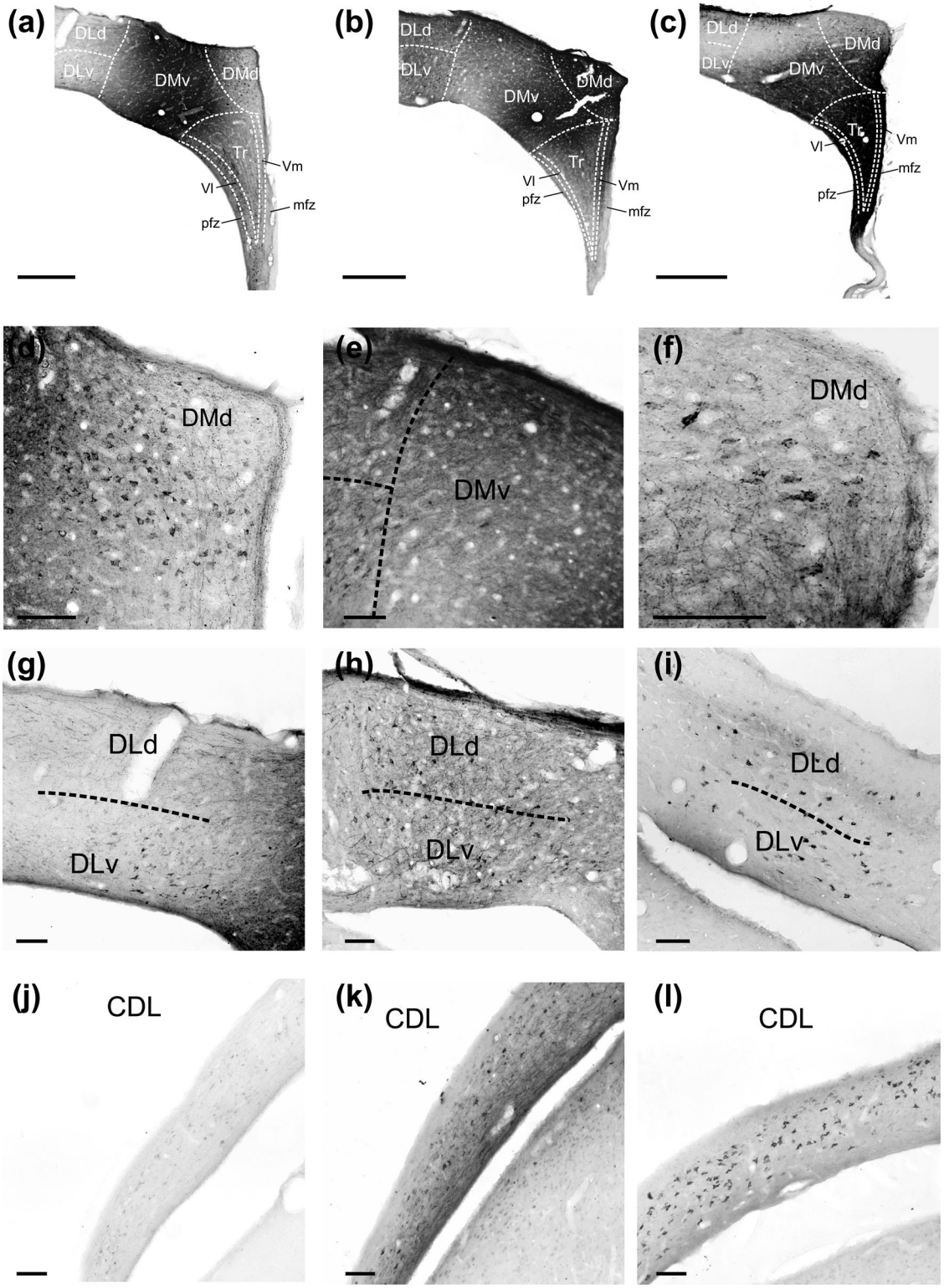

FIGURE 3 Dissociation of DM, DL, and CDL projections to the three injection groups. (a) In vivo injection into DMv. (b) In vivo injection into DMd, Tr, and medial DMv. (c) In vivo injection into the V-shaped area. (d) Retrogradely labeled neurons were found in DMd following DMv injections. (e) Fibers can be seen in the dorsal DMv after DMd/medial DMv injections. (f) Retrogradely labeled cells are visible in DMd after injections into the V-shaped area. (g) DMv injections resulted in retrogradely labeled cells in DLv, but not in DLd. (h) Both DL subareas (DLv and DLd) exhibit retrogradely labeled neurons after DMd/medial DMv injections. (i) V-shaped injections also labeled cells in DLv and DLd. (j) DMv injections lead to only sparse labeling in CDL. (k) Retrograde labeling in CDL following injections into DMd and medial DMv. (l) Retrograde labeling in CDL after injections into the V-shaped area. Scale bars represent 500 μm in panels (a–c) and 100 μm in panels (d–l).

10969861, 2023, 7, Downloaded from https://onlinelibrary.wiley.com/doi/10.1002/cne.25462 by Cochrane Germany, Wiley Online Library on [28/04/2023]. See the Terms and Conditions (https://onlinelibrary.wiley.com/terms-and-conditions) on Wiley Online Library for rules of use; OA articles are governed by the applicable Creative Commons License

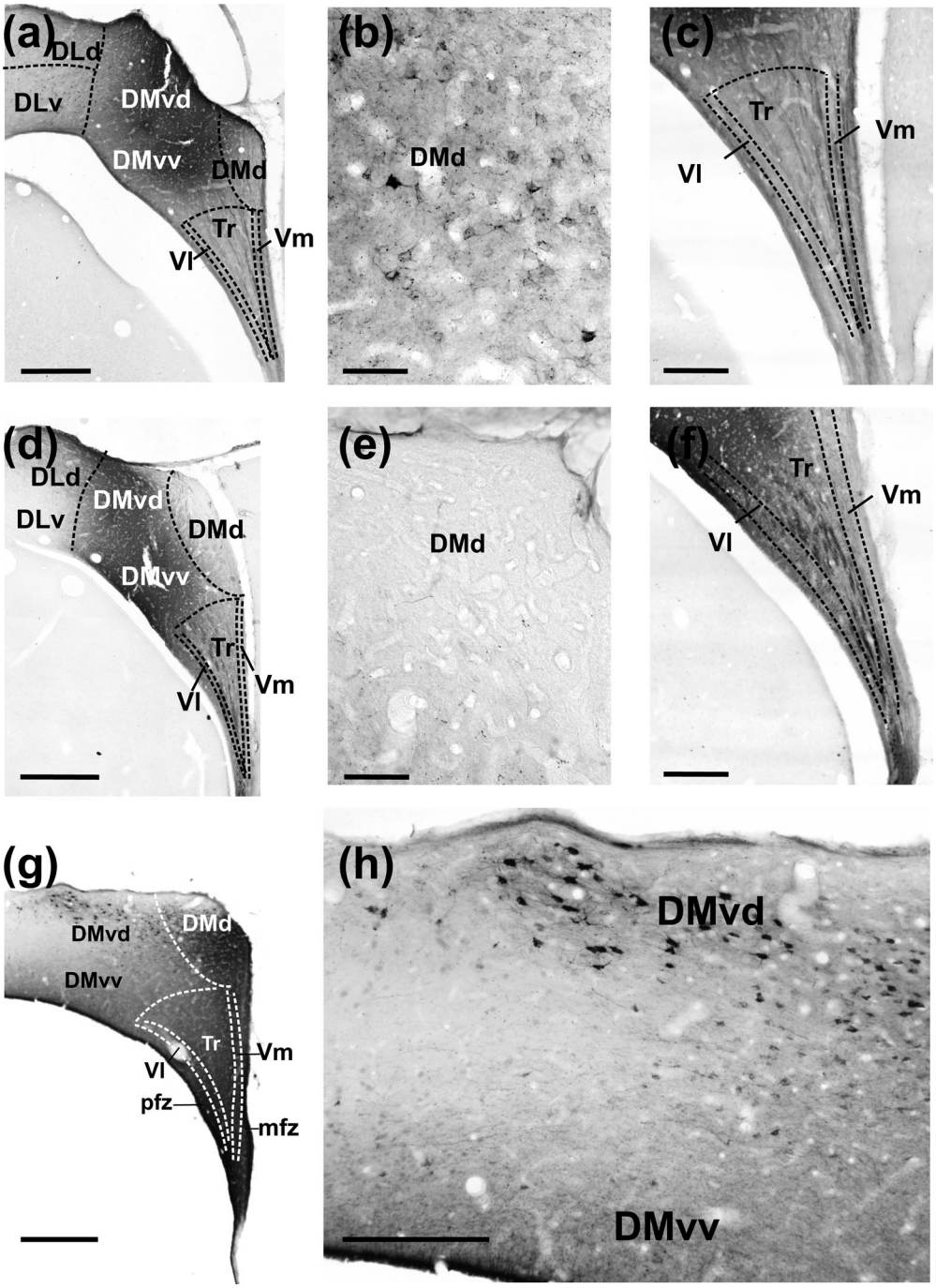

FIGURE 4 Different afferent inputs and efferent targets of DMvv and DMvd. (a) In vivo injection of tracer focused on DMvd. (b) Neurons in DMd were retrogradely labeled following DMvd injections. (c) DMvd injections mainly stained fibers running along medial Tr, Vm, and mfz. (d) In vivo injection of tracer focused on DMvv. (e) Injections that were prevailingly focused on DMvv did not label neurons in DMd. (f) DMvv injections resulted in labeling in lateral Tr, Vl, and pfz. (g) In vivo injection in the DMd and Vm. (h) Retrogradely labeled neurons can be observed in DMvd but not in DMvv. Scale bars represent 500 μm in panels (a, d, g); 50 μm in panels (b, e); and 250 μm in panels (c, f, h).

Finally, we stained hippocampal sections against DCX, which is a marker for adult neurogenesis (Figure 7). We found that DCX, similar to GFAP, was most strongly expressed in Vl (Figure 7c,f,i,l) and periventricular parts of DMvv (Figure 7b,e,h,k), while the dorsal subdivisions were nearly void of labeled cells (Figure 7). Similarly, CaMKIIα strongly stained the lateral V-shaped layer (Figure 8c,f,i,l) and DMvv (Figure 8b,e,h,k), but was also considerably expressed in other hippocampal subdivisions such as DMvd and DMd and to a lesser extent in Vm and Tr (Figure 8).

In sum, the expression of calbindin, GFAP, DCX, and CaMKIIα supports the subdivision of DMv into dorsal and ventral parts and are congruent with the deep versus superficial topography observed in

10969861, 2023, 7, Downloaded from https://onlinelibrary.wiley.com/doi/10.1002/cne.25462 by Cochrane Germany, Wiley Online Library on [28/04/2023]. See the Terms and Conditions (https://onlinelibrary.wiley.com/terms-and-conditions) on Wiley Online Library for rules of use; OA articles are governed by the applicable Creative Commons License

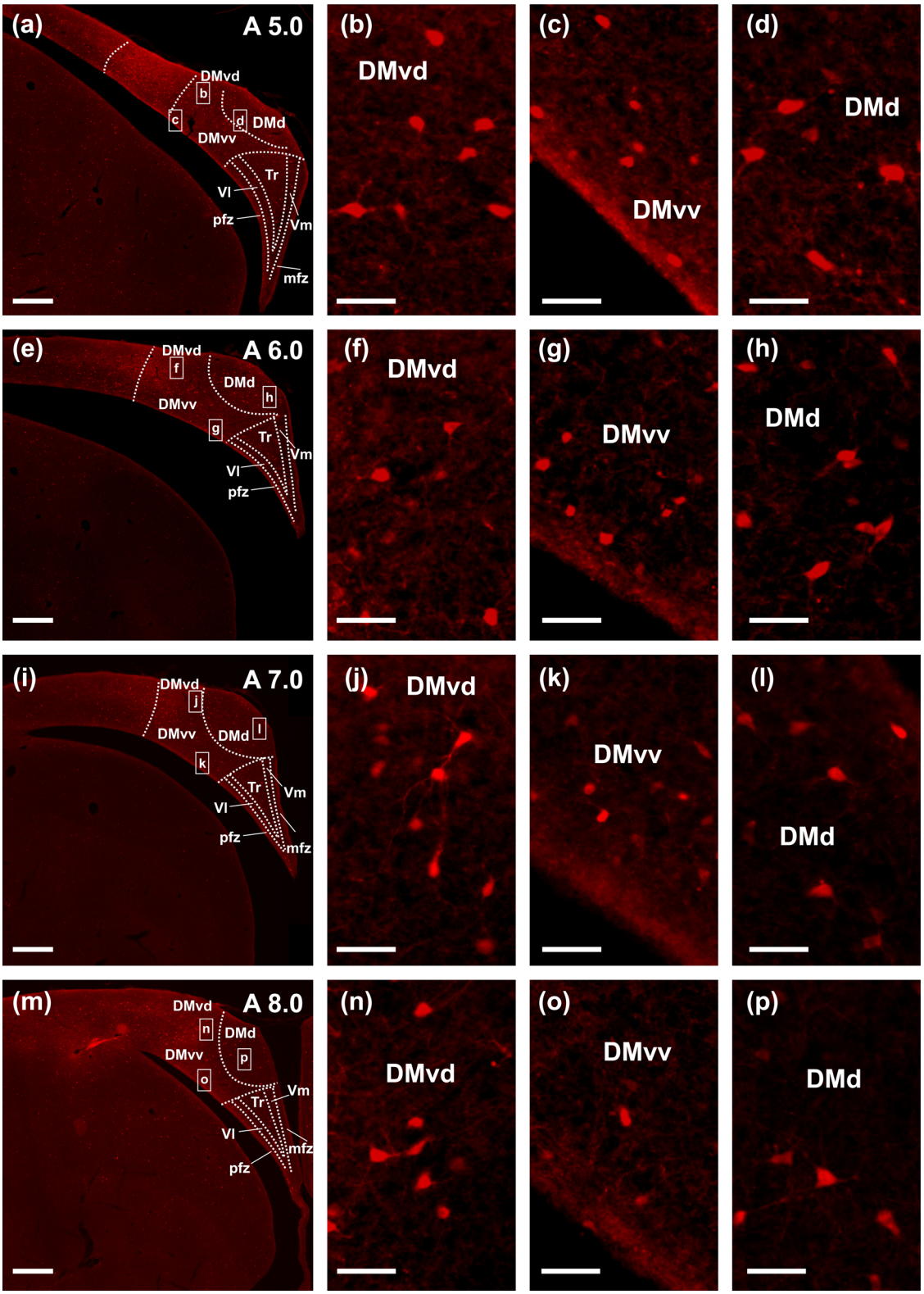

FIGURE 5 Neuronal expression of calbindin in the hippocampal formation (HF). (a, e, i, m) HF sections at different anterior posterior planes stained against calbindin. (b, f, j, n) A higher magnification image from the corresponding HF section focusing on calbindin-positive cells in DMvd. (c, g, k, o) A higher magnification image from the corresponding HF section focusing on calbindin-positive cells in DMvv. (d, h, l, p) A higher magnification image from the corresponding HF section focusing on calbindin-positive cells in DMd. Cells in dorsomedial areas are larger on average than cells in the ventrolateral region. Scale bars represent 500 μm in panels (a, e, l, m) and 50 μm in the higher magnification images.

10969861, 2023, 7, Downloaded from https://onlinelibrary.wiley.com/doi/10.1002/cne.25462 by Cochrane Germany, Wiley Online Library on [28/04/2023]. See the Terms and Conditions (https://onlinelibrary.wiley.com/terms-and-conditions) on Wiley Online Library for rules of use; OA articles are governed by the applicable Creative Commons License

JCN RESEARCH IN SYSTEMS NEUROSCIENCE THE JOURNAL OF COMPARATIVE NEUROLOGY WILEY

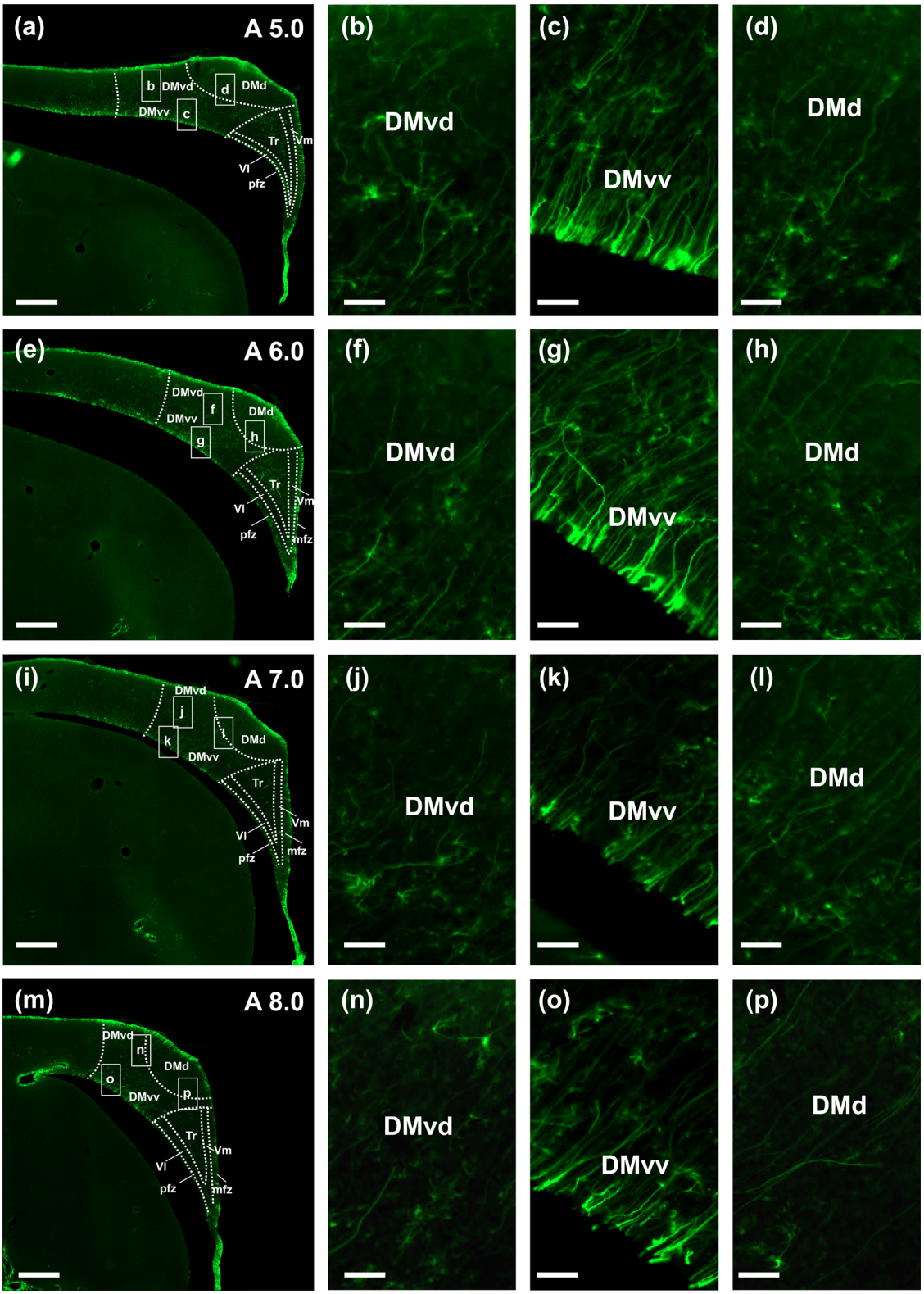

FIGURE 6 GFAP expression in the hippocampal formation (HF). (a, e, i, m) HF sections at different anterior posterior planes stained against GFAP. GFAP signal is observable throughout the HF. In the ventrolateral (deep) HF, the fluorescence signal can be seen mostly in fibers indicating the presence of radial glia, whereas in the dorsomedial (superficial) and central HF, GFAP is more abundant in astrocytes. (b, f, j, n) A higher magnification image from the corresponding HF section showing astrocytes in DMvd. (c, g, k, o) A higher magnification image from the corresponding HF section showing GFAP-stained fibers in DMvv. (d, h, l, p) A higher magnification image from the corresponding HF section showing astrocytes in DMd. Scale bars represent 500 μm in panels (a, e, i, m) and 50 μm in the higher magnification images.

10969861, 2023, 7, Downloaded from https://onlinelibrary.wiley.com/doi/10.1002/cne.25462 by Cochrane Germany, Wiley Online Library on [28/04/2023]. See the Terms and Conditions (https://onlinelibrary.wiley.com/terms-and-conditions) on Wiley Online Library for rules of use; OA articles are governed by the applicable Creative Commons License

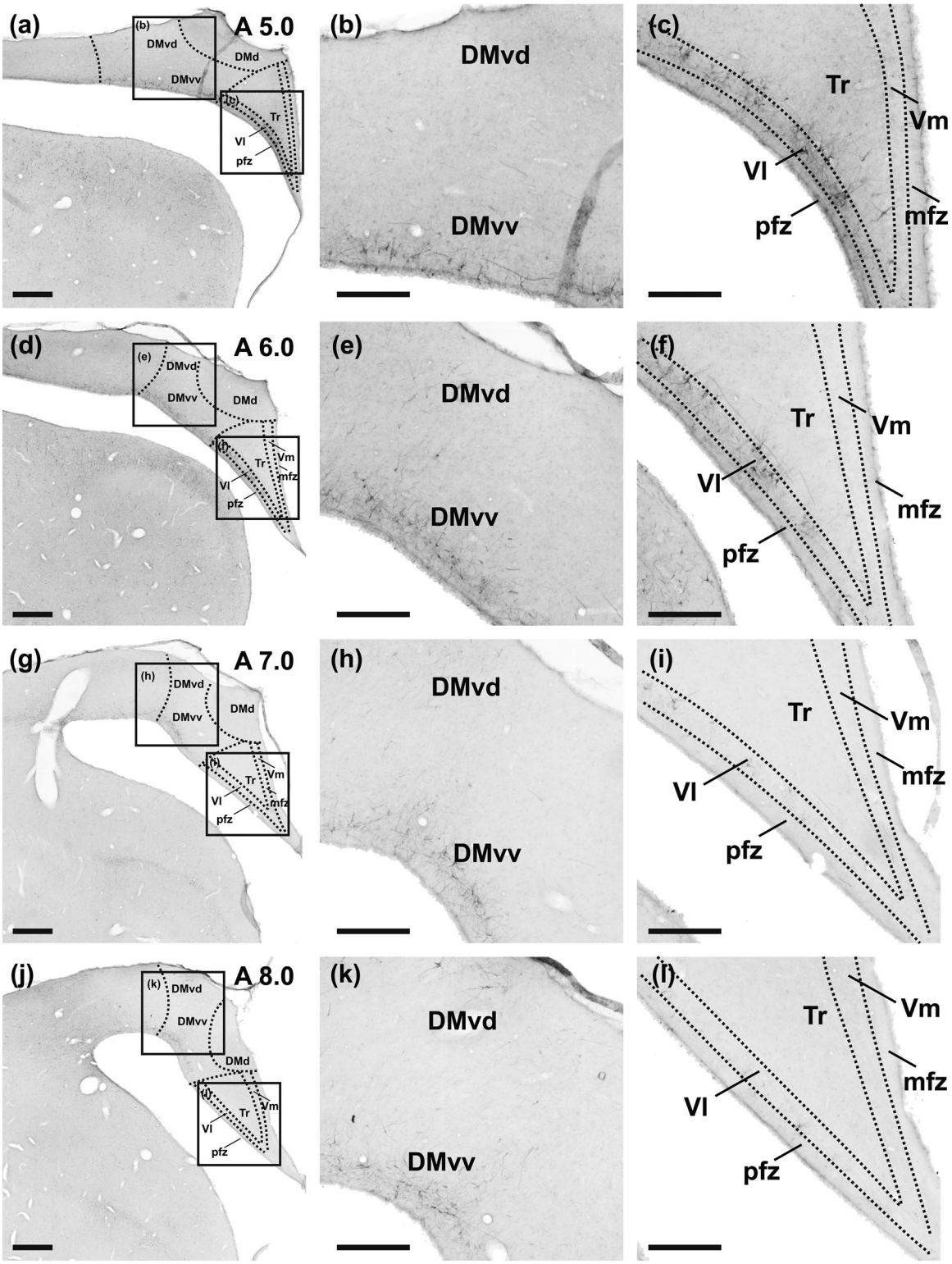

FIGURE 7 Expression patterns of DCX in the avian hippocampal formation (HF). (a, d, g, j) HF sections at different anterior–posterior planes stained against DCX. DCX expression can be mainly seen in Vl and DMvv. (b, e, h, k) A higher magnification image from the corresponding HF section focusing on DMvv and DMvd. (c, f, i, l) A higher magnification image from the corresponding HF section focusing on the V-shaped area. Scale bars represent 500 μm in panels (a, d, g, j) and 250 μm in the higher magnification images.

10969861, 2023, 7, Downloaded from https://onlinelibrary.wiley.com/doi/10.1002/cne.25462 by Cochrane Germany, Wiley Online Library on [28/04/2023]. See the Terms and Conditions (https://onlinelibrary.wiley.com/terms-and-conditions) on Wiley Online Library for rules of use; OA articles are governed by the applicable Creative Commons License

JCN RESEARCH IN SYSTEMS NEUROSCIENCE THE JOURNAL OF COMPARATIVE NEUROLOGY WILEY

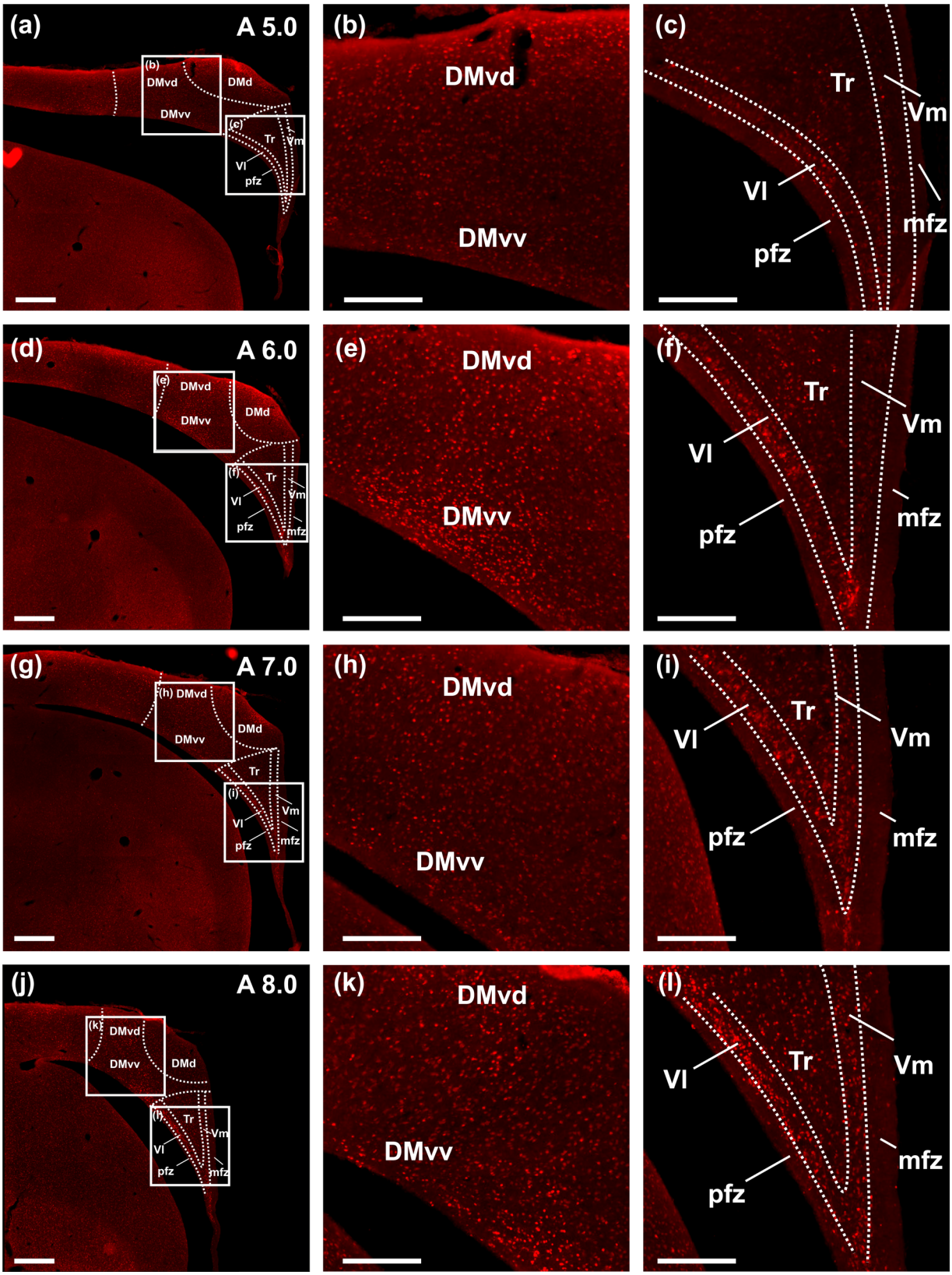

FIGURE 8 Expression patterns of CaMKIIα in the avian hippocampal formation (HF). (a, d, g, j) HF sections at different anterior–posterior planes stained against CaMKIIα. Expression is found in DMvv, DMvd, DMd, Vl, and Tr. However, expression is strongest in DMvv and Vl. (b, e, h, k) A higher magnification image from the corresponding HF section focusing on DMvv and DMvd. (c, f, i, l) A higher magnification image from the corresponding HF section focusing on the V-shaped area. Scale bars represent 500 μm in panels (a, d, g, j) and 250 μm in the higher magnification images.

10969861, 2023, 7, Downloaded from https://onlinelibrary.wiley.com/doi/10.1002/cne.25462 by Cochrane Germany, Wiley Online Library on [28/04/2023]. See the Terms and Conditions (https://onlinelibrary.wiley.com/terms-and-conditions) on Wiley Online Library for rules of use; OA articles are governed by the applicable Creative Commons License

our connectivity analysis. In addition, some of the markers (e.g., DCX, GFAP) indicate an even more subtle, possibly layered, subdifferentiation of the HF.

3.3 | In vitro injections

Our in vivo tracing data and marker expression patterns demonstrated differences between dorsomedial and ventrolateral hippocampal subdivisions and suggested that DMv needs to be further subdivided into a dorsal and ventral component. In order to investigate this segregation more thoroughly, in vitro tracings were performed that enable to target small subdivisions or small areas of the brain with greater precision. Therefore, brain slices were cut using a vibratome in continually oxygenated, ice-cooled sucrose-substituted Krebs solution. After that, biocytin crystals were applied to all hippocampal subdivisions in separate slices, which then were incubated in ACSF for 4 h.

3.4 | In vitro injections into DL

We first targeted DLd and DLv with biocytin crystals (Figure 9). DLd injections resulted in many fibers that ran through DMvd and DMd and continued along the mfz as well as the medial Tr (Figure 9a,b). A few of these fibers showed varicosities and, on occasion, exhibited both medially and laterally oriented collaterals within Tr (Figure 9b,c). These fibers were mostly confined to the medial half of Tr and only a small number of collateral branches extended further laterally. In addition, a bunch of fibers was typically observed along the dorsomedial pial surface. Most of these fibers were quite thick and on occasion exhibited varicosities (Figure 9b,d). While these fibers descended toward the septum, some collaterals branched off in DMd, whereas only very few were found in Vm or Tr. In addition, many retrogradely labeled neurons could be found in DMd (Figure 9d), while labeled neurons were only rarely seen in DMv.

In contrast, after crystal placement in DLv varicose fibers were labeled in DMvv (Figure 9e,g), with some of these fibers also reaching Vl (Figure 9f). Furthermore, neurons labeled in DLv formed a thick plexus of dendrites and axons, which extended to the dorsal most parts of DLd, perpendicular to the pial surface (Figure 9h).

3.5 | In vitro injections into DM

In vitro experiments with injections into DM showed a topographical pattern of projections similar to that found in the in vivo experiments. When crystals were placed in DMv, the resulting projection patterns also suggested a separation into a dorsal (DMvd) and a ventral (DMvv) area. Injections focused on DMvd revealed fibers traversing dorsally in the HF through DMd and mfz (Figure 10a–f). These fibers exhibited some varicosities near the injection site and DMd, while the most medial part of DMd showed few to no varicosities (Figure 10b,e). Fibers that continued to mfz could be tracked to Vm, whereas the fibers that crossed DMd could not be tracked further as they appeared to run through other anterior–posterior planes. In contrast, injections focused on DMvv labeled fibers that ran through the ventral HF including Vl, the lateral part of Tr and pfz (Figure 10g,h). These fibers showed many varicosities indicating putative contacts to lateral Tr and Vl neurons (Figure 10h). Hence, it seems that the main projection target of the DMvd within the HF could be the DMd, whereas the projection targets of DMvv seem to be Vl and the lateral Tr. Both DMv subareas furthermore seem interconnected with each other. In addition, the neurons in DMvv and DMvd were arranged such that their long dendrites span the dorsoventral extent of the HF toward the pial and ventricular surface, respectively (Figure 10c,i).

When crystals were placed in DMd, labeled fibers were found throughout the medial and central part of Tr (Figure 10j,k), which exhibited an abundance of varicosities that appeared to contact Tr and Vm neurons (Figure 10j,k).

Together, the data suggest that DM neurons send projections along the dorsolateral/ventromedial curvature of the HF in parallel with the transverse axis. In many cases, DM connections were reciprocal, as retrogradely labeled neurons were observable in DMd following DMvd injections (Figure 10b) and labeled neurons were found in central and medial Tr following DMd injections (Figure 10j,k).

3.6 | In vitro injections into the V-shaped area

In the next step, we analyzed in vitro injections within the V-shaped area. Tr injections resulted in strong projections to DMv, especially DMvv, although not to DMd (Figure 11a,b). Interestingly, Tr neurons gave rise to long dendritic trees expanding across Vm and extending up to the mfz where they crossed with orthogonally running fibers of this fiber zone (Figure 11c). Furthermore, many fibers from Tr injection site left the HF in a ventral direction (Figure 11a).

Vm injections revealed projections to DMd, Vl, and Tr (Figure 11d–g). On the one hand, labeled fibers were observed to run dorsally along the mfz to innervate the DMd (Figure 11d,e). On the other hand, some fibers were also found to traverse through the Tr, many reaching the Vl and the pfz (Figure 11d,f,g). A lot of these fibers contained varicosities, indicating that they might contact neurons in Tr on their way to Vl. Furthermore, within the medial Tr, some retrogradely labeled neurons could be seen close to Vm (Figure 11f). It is possible that these were labeled due to their dendrites extending into Vm or due to tracer spread. In one of these cases, the axon of such a neuron could be followed toward the lateral Tr; however, the termination area of this axon could not be determined precisely. Nevertheless, the observed labeling pattern opens the possibility that there might be a form of intrinsic circuitry that connects the lateral and medial parts of Tr.

In a similar fashion, Tr was the main target of Vl projections as a large number of fibers could be found in this subregion after biocytin placement into Vl (Figure 11h–j). Some fibers were also observed to be headed toward DMv. A fiber bunch was also seen in the pfz that left the HF ventral to the injection site.

10969861, 2023, 7, Downloaded from https://onlinelibrary.wiley.com/doi/10.1002/cne.25462 by Cochrane Germany, Wiley Online Library on [28/04/2023]. See the Terms and Conditions (https://onlinelibrary.wiley.com/terms-and-conditions) on Wiley Online Library for rules of use; OA articles are governed by the applicable Creative Commons License

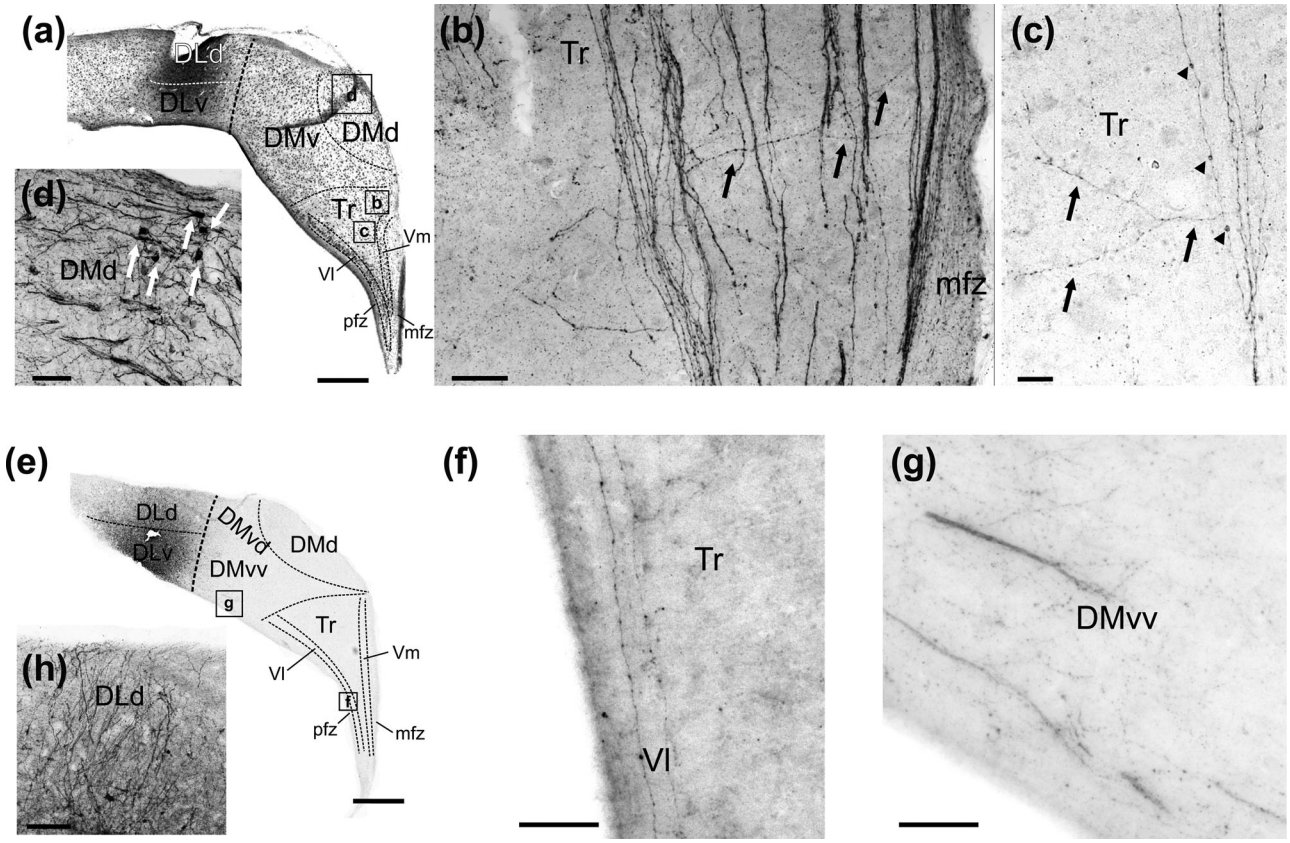

FIGURE 9 Different projection patterns from the ventral and dorsal DL. (a) A section of the hippocampal formation (HF) where a biocytin crystal had been positioned onto DLd. (b) Fibers traversing DMd and medial Tr in the dorsomedial HF, from where occasional collateral branches sprouted that ran medially (black arrows). (c) These fibers often showed large varicosities (arrow heads). Collateral fibers could also be found to branch off toward the lateral HF (black arrows). (d) Retrogradely labeled neurons could frequently be observed in DMd following crystal placement in DLd. (e) A section where the crystal placement was performed in DLv. (f) DLv crystal placement resulted in fibers in the ventrolateral part of the HF, some reaching Vl. (g) Fibers could also be seen in DMvv after DLv injections. (h) Dendrites and axons in DLd from DLv neurons extending perpendicular to the pial surface. Scale bars represent 500 μm in panels (a, e), 100 μm in panel (h), 50 μm in panels (b, d, f, g), and 20 μm in panel (c).

4 | DISCUSSION

The aim of the present study was to gain a deeper understanding of the connectivity pattern within the HF of homing pigeons. To this end, we traced the connectivity among the neurochemically defined subdivisions of HF (Herold et al., 2014) using in vivo and in vitro tracing methods. Most previous avian hippocampal tracing studies have used in vivo injections and traced the three major subdivisions DL, DM, and the V-shaped area (Atoji & Wild, 2004; Kahn et al., 2003). However, recent anatomical (Abellán et al., 2014; Herold et al., 2014; Medina et al., 2017; Redies et al., 2001) and functional (Payne et al., 2021) evidence suggests that this low-resolution subdivisional scheme does not capture numerous subdivisions that collectively form DL, DM, and the V-shaped area, especially along the hippocampal transverse axis. Tracing the connectivity of smaller subdivisions is only possible with in vitro tracing that offers a high spatial specificity, such as the use of small biocytin crystals that can be applied to brain slices that are artificially kept alive. By using biocytin, we were therefore able to investigate, for example, the connections of the small V-shaped layers, whose connectivity has only been previously inferred from retrograde labeling (Kahn et al., 2003).

4.1 | Intrahippocampal connectivity

Overall, we found that the avian HF comprises several reciprocal connections among subdivisions and could confirm connections that have already been established in previous tracing experiments (Atoji & Wild, 2004; Kahn et al., 2003) and with resting-state fMRI (Behroozi et al., 2017). For example, we found that DM is reciprocally connected with Tr, the V-shaped layer, and DL. Likewise, we saw that DL has reciprocal connections with DM and Tr.

Using in vitro tracings, we could reveal in much more detail the patterns of connectivity among smaller subdivisions and found that at least two parallel pathways can be distinguished within the avian HF: a more dorsomedial (superficial) and a more ventrolateral (deep) pathway. In the superficial pathway, DLd sends efferents to DMd and medial Tr, and to a lesser extent to Vm. DMd in turn projects to Vm and

10969861, 2023, 7, Downloaded from https://onlinelibrary.wiley.com/doi/10.1002/cne.25462 by Cochrane Germany, Wiley Online Library on [28/04/2023]. See the Terms and Conditions (https://onlinelibrary.wiley.com/terms-and-conditions) on Wiley Online Library for rules of use; OA articles are governed by the applicable Creative Commons License

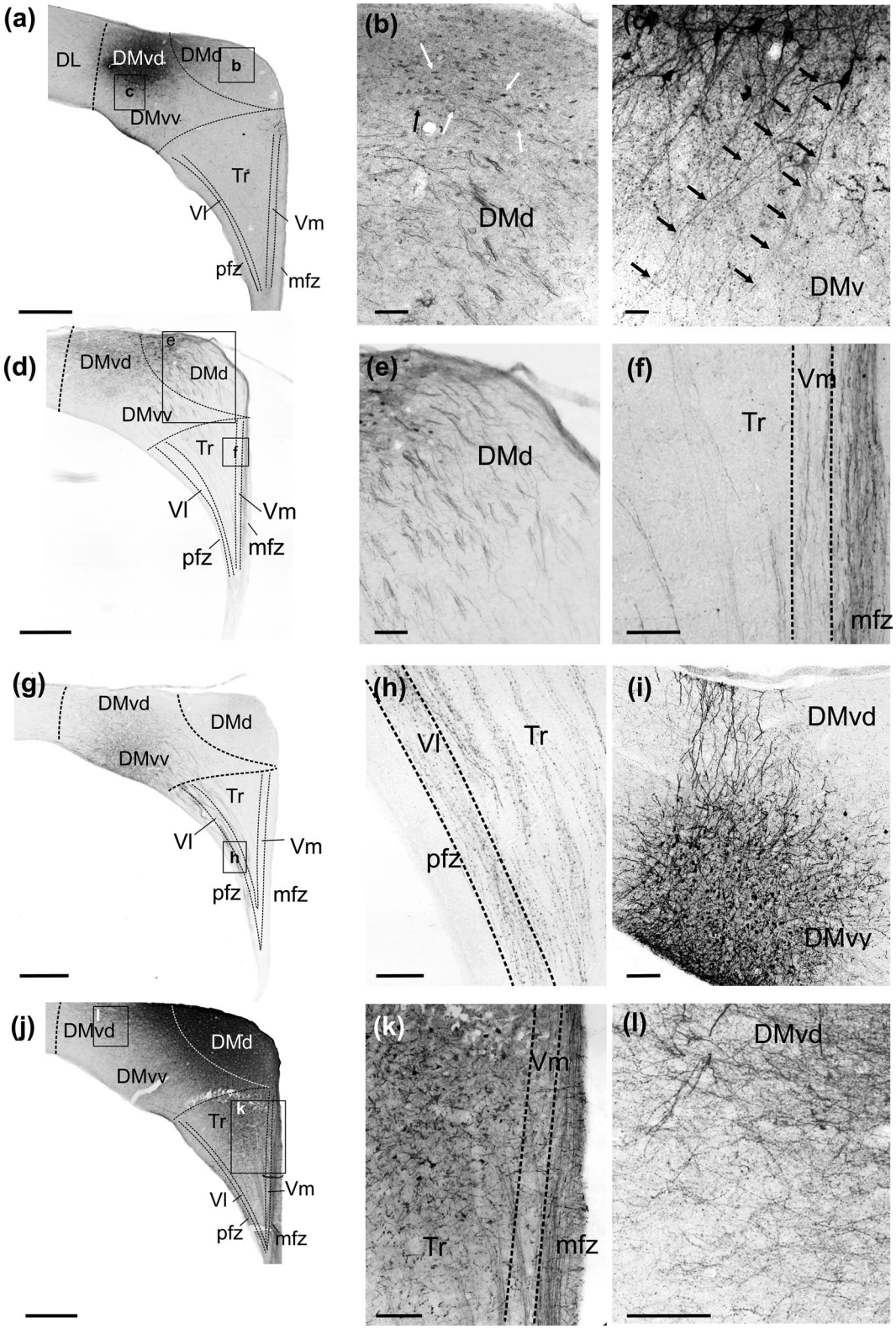

FIGURE 10 Contrasting projection patterns of DMvd, DMvv, and DMd. (a) A section with biocytin crystal placement into DMvd. (b) Neurons and fibers are labeled in DMd after DMvd injection. Some varicose fibers are highlighted with black arrows, and white arrows indicate examples of neurons with retrograde labeling. (c) Magnification of a neuron within DMvd extending its dendrites (black arrows) down to the periventricular border. (d) Slice showing the injection site that included the medial part of DMvd and the lateral aspect of the DMd. (e) Neurons and fibers are labeled in DMd after DMvd injection. (f) Injections into the medial part of DMvd result in fibers running across the central Tr and mfz. (g) A section where a biocytin crystal was placed into DMvv. (h) Following DMvv injections, fibers were observed in lateral Tr and Vl. (i) Dendrites from DMvv neurons extending to DMvd. (j) A section with biocytin crystal placement in DMd. (k) Medial Tr exhibited labeled neurons and fibers after DMd

(Continues)

10969861, 2023, 7, Downloaded from https://onlinelibrary.wiley.com/doi/10.1002/cne.25462 by Cochrane Germany, Wiley Online Library on [28/04/2023]. See the Terms and Conditions (https://onlinelibrary.wiley.com/terms-and-conditions) on Wiley Online Library for rules of use; OA articles are governed by the applicable Creative Commons License

FIGURE 10 (Continued)
injections. Fibers could also be seen throughout Vm and mfz. (l) DMd injections led to anterograde labeling in DMvd. Scale bars represent 500 μm in panels (a, d, g, j); 100 μm in panels (e, i, k, l); 50 μm in panels (b, f, h); and 20 μm in panel (c).

medial Tr, as well as back to DLd. DMd also has reciprocal connections to DMvd. Finally, Vm sends projections to Vl and Tr.

In the deep pathway, DLv mainly projects to DMvv, but it is also weakly connected to Vl. From DMvv, efferents are sent to Vl and lateral Tr. Vl sends projections back to DMvv and Tr. Lastly, DMd and DMvv receive projections from the medial and lateral portions of Tr, respectively. The superficial and the deep pathways are interconnected in DL and DM, as well as in the V-shaped area through connections between lateral and medial Tr (Figure 12).

Overall, our findings are consistent with a feedforward circuit of the avian HF that has been proposed in earlier studies (Hough et al., 2002; Kahn et al., 2003). These studies suggested that information flow starts in DL, from where information is relayed to DM. DM then projects to Vm, from where information reaches the Vl, which finally projects back to DM, which in turn projects out of the HF (Hough et al., 2002; Kahn et al., 2003). In the current study, we found an overall similar projection pattern. However, importantly, our higher spatial–anatomical resolution biocytin data indicate the presence of two anatomically dissociable hippocampal pathways, a dorsomedial (superficial) and a ventrolateral (deep) pathway, along the hippocampal transverse axis.

The presence of hippocampal parallel processing streams along the transverse axis is already apparent in DL, as DLd showed rather dorsomedial and DLv ventrolateral projection patterns. Although not intentionally targeting DLv and DLd with anterograde tracers, Atoji and Wild (2004) already proposed a separation of DL into dorsal and ventral regions when they reported neurons in DLv and fibers in DLd after injection into DM. We observed the same pattern in our in vivo data and could further show with in vitro tracings that the fibers in DLd mainly arise from the DMvd and DMd. However, our in vitro injections into DLd consistently labeled neurons within the DMd, but not DMvd, suggesting a stronger projection from DMd to DLd. Overall, our findings are consistent with the previously described connectivity of DL (Atoji & Wild, 2004). Similarly, we found that projections originating from DM were topographically organized. While tracer injections into DMvv resulted mainly in labeling in Vl, tracer injections into DMvd and DMd mainly resulted in labeling in Vm and medial Tr. Previous studies did not subdivide DMv into pathway-dissociable ventral and dorsal regions. However, our tracings as well as our immunohistochemical results suggest that DMv is a heterogeneous HF area that can be subdivided into a dorsal (DMvd) and ventral (DMvv) component. Although earlier studies did not explicitly trace the dorsal and ventral components of DM, their findings support our partitioning of DMv (Atoji & Wild, 2004; Kahn et al., 2003). For example, Kahn et al. (2003) report that CTB injections into the part of DM that we consider DMvv stained neurons within Vl, while injections into the medial DM, which corresponds to our DMd, led to anterogradely labeled fibers as well as retrogradely labeled neurons in Vm. Moreover, Atoji and Wild (2004, 2005) found retrogradely labeled neurons within Vl after lateral DM injections, and labeled Vm neurons following medial DM injections. It is possible that the mediolateral topography described by Atoji and Wild (2004) is partly comparable to our parallel dorsomedial–ventrolateral topography because of the curvature of the hippocampal transverse axis. However, it is also possible that a mediolateral topography as described by Atoji and Wild (2004) is a distinctive property of DMv as some studies found medial/lateral differences in DMv with respect to its connectivity with CDL (Atoji & Wild, 2005), hyperpallium densocellulare, and cortex piriformis (Kahn et al., 2003). In this regard, it is interesting to point out that cadherins and calcium-binding proteins revealed radial hippocampal subdivisions in chickens (Redies et al., 2001; Suárez et al., 2006) that might fit well with the idea of mediolateral differences within DM. The intermediate subdivision of the parahippocampal area (APHi), which might approximately correspond to the lateral DM in Atoji and Wild (2004), is distinguishable from that of the medial parahippocampal area (APHm) that could, with some caveats, roughly correspond to the medial DM. Moreover, the APHi displays further lateral–medial subdifferentiation (Suárez et al., 2006). The DMvd in our study might include the superficial part of the APHi, or at least its medial aspect (APHim). By contrast, the DMvv might correspond to the deep part of the (medial) APHi together with aspects of the deep part of APHm. Thus, further studies are needed to determine if and how these different topographies relate to each other, preferably leading to a unified terminology.

Moreover, we found that information from both V-shaped layers is further conveyed to Tr and that focal injections into Vm gave rise to fibers targeting Vl. The Vm to Vl connection has previously been suggested based on electrophysiological (Hough et al., 2002) and anatomical data (Kahn et al., 2003). However, previous in vivo retrograde and anterograde tracer injections into Vl and Vm, respectively, contained tracer spread in Tr and DM; therefore, the conclusions about this connection remained putative (Kahn et al., 2003). Nevertheless, we now confirmed this projection with focal in vitro anterograde tracings.

It is noteworthy that the intrahippocampal circuitry also includes connectivity between the left and right HF. Particularly interesting is that contralateral connections display a topographic pattern along the rostrocaudal axis (Atoji et al., 2002). Contralaterally projecting zones possibly include parts of DL and DM, as well as Vl and Vm (Atoji et al., 2002; Casini et al., 1986; Kahn et al., 2003). Additionally, it seems that some of the contralateral connections resemble the ipsilateral patterns of connectivity; for example, tracer injection into ventral regions including parts of DMvv and DLv resulted in retrogradely labeled neurons in the contralateral Vl (Kahn et al., 2003). On the other hand, tracer injection involving mainly Vl, lateral Tr, and possibly parts of DMvv revealed a retrogradely labeled group of cells within the contralateral DMd (Kahn et al., 2003), and anterograde and retrograde tracings suggest that Vm projects to the contralateral Vl (Atoji et al., 2002; Kahn et al., 2003).

10969861, 2023, 7, Downloaded from https://onlinelibrary.wiley.com/doi/10.1002/cne.25462 by Cochrane Germany, Wiley Online Library on [28/04/2023]. See the Terms and Conditions (https://onlinelibrary.wiley.com/terms-and-conditions) on Wiley Online Library for rules of use; OA articles are governed by the applicable Creative Commons License

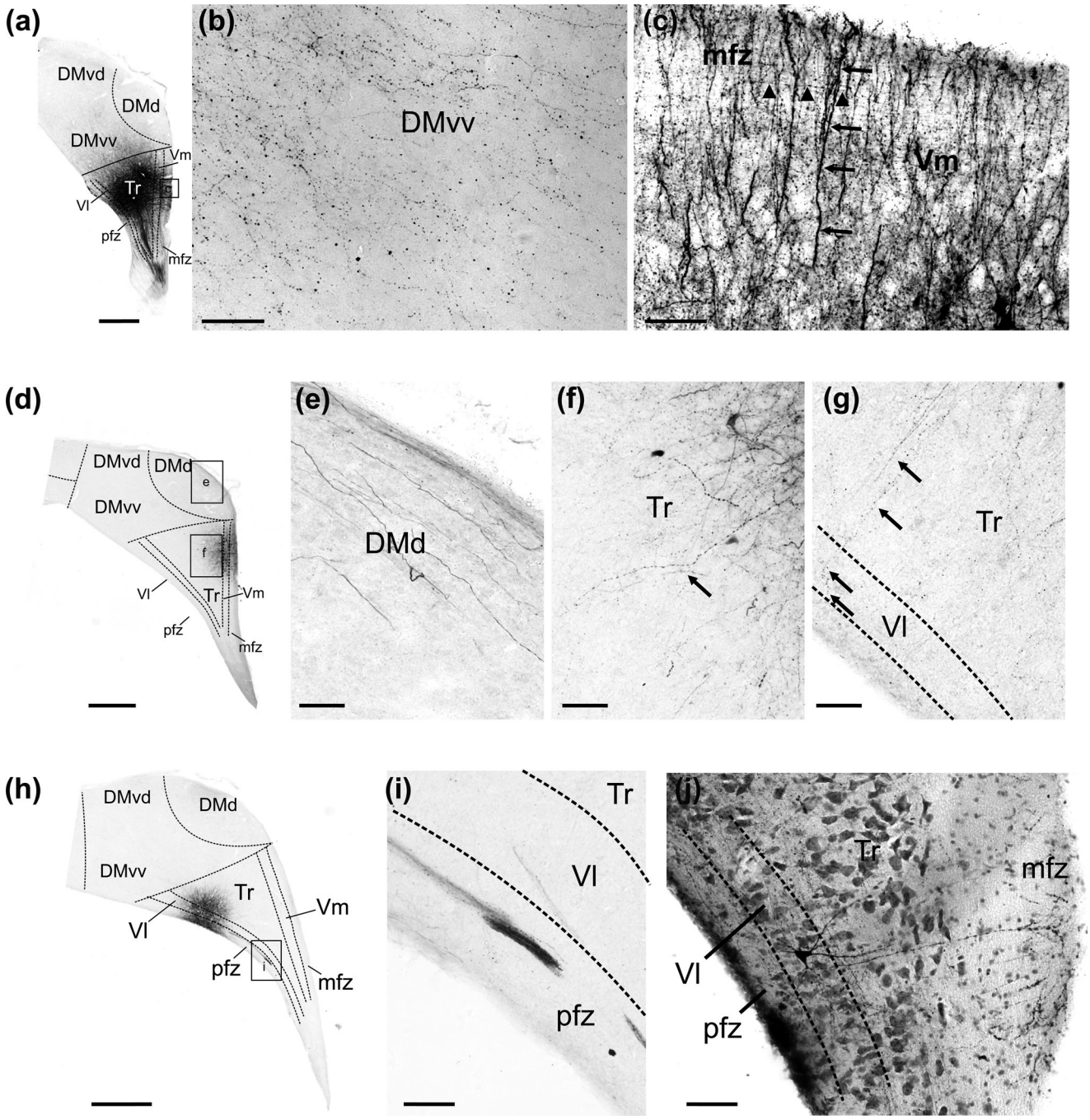

FIGURE 11 Intrinsic connectivity of the V-complex. (a) A section with the biocytin placed in Tr. (b) Many fibers can be seen in DMvv after Tr injection. (c) Dendrites of Tr neurons (black arrows) extend medially toward mfz in a parallel fashion and orthogonal to the fibers running through the mfz (black arrowheads). (d) A section with biocytin placement into Vm. (e) Fibers and terminal-like varicosities were labeled in DMd after Vm injections. (f) Higher magnification image of fibers in Tr with varicosities following Vm injection. Black arrow points to an example of a varicose fiber. (g) Fibers crossing Tr and reaching Vl and pfz after injection into Vm (arrows). (h) A section with injection into Vl. (i) Dense fiber bundles could be observed in the pfz following Vl injections. (j) Labeled fibers within Tr, Vl, and pfz after Vl injections. The section also shows an example of a neuron located in Vl with dendritic arborization that extend across Tr to Vm and the mfz. Scale bars represent 500 μm in panels (a, d, h) and 50 μm in panels (b, c, e, f, g, i, j).

10969861, 2023, 7, Downloaded from https://onlinelibrary.wiley.com/doi/10.1002/cne.25462 by Cochrane Germany, Wiley Online Library on [28/04/2023]. See the Terms and Conditions (https://onlinelibrary.wiley.com/terms-and-conditions) on Wiley Online Library for rules of use; OA articles are governed by the applicable Creative Commons License

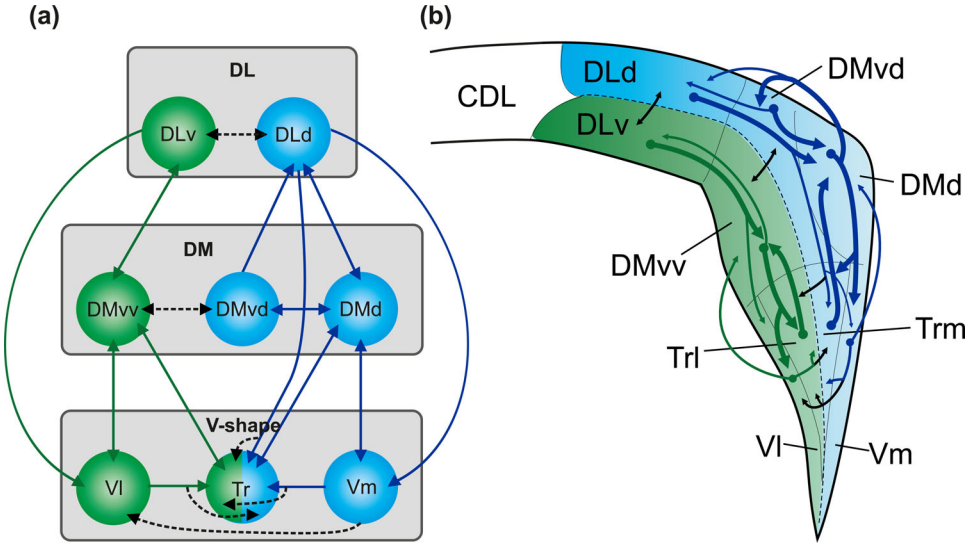

FIGURE 12 Avian hippocampal pathways. (a) Summary of all connections that were found in the hippocampal in vivo and in vitro tracings. The projections within the HF are topographically organized along the transverse axis. Structures belonging to the dorsomedial (superficial) pathway are highlighted in blue and structures belonging to the ventrolateral (deep) pathway are highlighted in green. Integration of information in the two pathways occurs at different anatomical levels (black lines). (b) In vitro and in vivo data presented on a section of the hippocampal formation. The projections within the HF are topographically organized along the transverse axis, and the dorsomedial and ventrolateral pathways are depicted in blue and green, respectively. Denser projections that appeared to be stronger, suggesting a core hippocampal circuit, are depicted with thicker lines. In brief, in the superficial pathway (blue), DLd sends efferents to DMd and medial Tr (Trm), and to a lesser extent Vm. DMd in turn projects to Vm and Trm, as well as sends a reciprocal projection back to DLd. DMd also has reciprocal connections to DMvd. Finally, Vm sends information to Vl and Tr. In the deep pathway (green), DLv mainly projects to DMvv but also weakly to Vl. From DMvv, efferents are sent to Vl and lateral Tr (Trl). Vl sends projections back to DMvv and Tr. Lastly, DMd and DMvv receive projections from the medial and lateral portions of Tr, respectively. The dorsal and the ventral pathways are interconnected in DL, in DM, and in the V-shaped area through connections between lateral and medial Tr.

4.2 | The distinction between the dorsomedial and ventrolateral pathway

Our findings indicate that the avian HF can be subdivided into two streams along its transverse axis. This finding is in line with recent electrophysiological, neurochemical, and functional data of the avian HF. For example, Payne et al. (2021) investigated SWRs across the hippocampal transverse plane in tufted titmice (*Baeolophus bicolor*). They found that the sharp wave component inverted from a positive to a negative polarity between dorsal and ventral recording sites. Moreover, they reported that the current source density was structured along the radial axis as they found a current source dorsal to a sink, concluding that SWRs exhibit a laminar organization in the HF of the titmouse. In the mammalian HC, SWRs also show a laminar distribution of sinks and sources (Ylinen et al., 1995) and are typically thought to be the result of a dense pyramidal cell layer with parallel dendrites, which give rise to large local field potential fluctuations through the summation of smaller currents (Buzsáki, 2015). More specifically, SWRs occur when clusters of pyramidal cells are spontaneously active leading to a summation of activity within the CA3 network, driving reciprocally connected interneurons to create the phase-locked, ripple-frequency spiking (Schlingloff et al., 2014). Payne et al. (2021) concluded that avian SWR might result from a more subtle laminar organization of cells, as no clear layering is visible in avian HF, or from other characteristics of hippocampal organization along the radial axis, such as differences in synaptic input (Valero et al., 2015), morphology (Montagnese et al., 1993), or intrinsic cell properties (Montagnese et al., 1996).

The pattern of HF connections found in our study could provide a network that is able to produce similar SWRs. We found that avian HF contains several reciprocal circuits as the two pathways along the transverse axis are characterized by strong feedback projections that occur at many regional subdivisions. Moreover, the two pathways are connected to each other at many subdivisional areas via direct projections, as well as via neurons that are aligned orthogonally to the transverse axis and extend their dendrites across the HF. These dendrites reach the fiber bundles that course through the HF dorsally and ventrally, potentially enabling the integration of their inputs. Our tracing data are in line with early studies characterizing hippocampal neurons in chicks and pigeons (Tömböl, Davies, Németh, Alpár, et al., 2000; Tömböl, Davies, Németh, Sebestény, et al., 2000) showing that hippocampal projection neurons give rise to recurrent collaterals that extend in the dorsoventral and mediolateral plane, possibly contacting other excitatory and inhibitory hippocampal neurons. Overall, the data from the current study and other data suggest that the avian HF contains a complex intrinsic network suitable to sustain and modulate incoming neural activity by a recurrent neural network. This proposed recurrent network could be a potential oscillation-producing system capable of generating SWRs.

The overall dorsomedial/ventrolateral separation observed in our tracings stands seemingly in contrast to the nonlaminar appearance

10969861, 2023, 7, Downloaded from https://onlinelibrary.wiley.com/doi/10.1002/cne.25462 by Cochrane Germany, Wiley Online Library on [28/04/2023]. See the Terms and Conditions (https://onlinelibrary.wiley.com/terms-and-conditions) on Wiley Online Library for rules of use; OA articles are governed by the applicable Creative Commons License

of the avian HF. More recent evidence suggests, however, that the avian HF displays a laminar organization (Abellán et al., 2014; Fujita et al., 2022; Redies et al., 2001). For instance, a subset of serotonergic receptors is expressed in a laminar fashion in 1-day-old chickens (Fujita et al., 2022). Similarly, laminar expression patterns of cadherins were observed in embryonic chick brain tissue (Redies et al., 2001). These layers are organized orthogonal to the orientation of radial glia (Abellán et al., 2014) and can be visualized with staining against calcium-binding proteins, neuronal nitric oxide synthase, and GABA in adult chicken (Suárez et al., 2006). Based on this finding, it was suggested that the ventral and dorsal subdivisions of the avian DL might correspond to deep versus superficial hippocampal layers in mammals, respectively (Medina et al., 2017). Our data confirm the presence of a laminar arrangement, which is not restricted to DL but continues along the whole transverse axis as we find topographic projections between dorsomedial (superficial) and ventrolateral (deep) subdivisions of the avian HF.

The distinction between dorsomedial and ventrolateral HF observed in our study might also reflect functional differences. For example, some studies suggest that the dorsomedial HF might play a special role in spatial memory as remembering locations of cached food, based on spatial cues, preferentially activated the superficial, but not the deep region of the HF (Mayer & Bischof, 2012; Mayer et al., 2010). In contrast, the deep HF of female zebra finches was preferentially activated when birds listened to the directed song of males (Bailey et al., 2002). Overall, these studies support the hypothesis of a functional segregation along the transverse axis that would be consistent with our anatomical findings. Future, functional studies of the avian HF should focus on investigating superficial/deep differences in hippocampal function.

4.3 | The segregation of DMv into DMvd and DMvv

Another main finding of our study that is consistent with the overall segregation of HF into numerous subdivisions aligned along two parallel processing streams is that DMv can be further subdivided into a dorsal (DMvd) and a ventral (DMvv) region. This distinction was not only seen in projection patterns of DMvv and DMvd, but also in the expression of some of our immunohistochemical markers. For example, staining against calbindin revealed morphological differences as calbindin-positive cells in DMd and DMvd were larger compared to cells in DMvv. Similar results were reported for two food-storing (marsh tit [*Parus palustris*] and magpie [*Pica pica*]) and two nonstoring (great tit [*Parus major*] and jackdaw [*Corvus monedula*]) species of birds (Montagnese et al., 1993). Montagnese et al. (1993) found larger neurons in the dorsomedial HF compared to other hippocampal subdivisions in all four species. Moreover, the calbindin-positive neurons within the dorsomedial HF were significantly larger in the food-storing species compared to the nonstorers, suggesting a specialized role of the dorsomedial HF in spatial tasks.

Moreover, the distinction between DMvv and DMvd could be observed in our GFAP staining. In general, GFAP is widely used as a marker for astrocytes, but it is also used to stain radial glia (Sievers et al., 1992). In our case, we found that the GFAP staining labeled a thin cell layer along the pial surface of the HF as well as cells located in the periventricular area of DMvv and DL, which were characterized by dense radial processes that seemed weaker in DMvd and DMd. Furthermore, a band of astrocytes was usually observed reaching from DMv to Tr. Thus, the GFAP staining might support the segregation of DMv into dorsal and ventral subdivisions. It is generally assumed that the main function of radial glia is to act as scaffolding during neuronal migration. However, in the DG of adult mammals, radial glia also acts as a precursor for differentiating neurons and glia cells (Casper & McCarthy, 2006; Garcia et al., 2004). Astrocytes within the mammalian HC are associated with memory processes (Adamsky et al., 2018), encode reward location (Doron et al., 2022), and modulate hippocampal–cortical communication during learning (Kol et al., 2020). More specifically, astrocytes in CA1 encode spatial information that complements place cell spatial encoding (Curreli et al., 2021). If astrocytes were to serve similar functions in birds, our observed pattern could indicate a functional segregation within the avian HF.

4.4 | Comparison to the mammalian HF

The question of homology between the avian and mammalian hippocampal subdivisions continues to be intensely debated (Atoji & Wild, 2004; Atoji et al., 2016; Erichsen et al., 1991; Kahn et al., 2003; Siegel et al., 2002; Szkely & Krebs, 1996). Some authors share the view that, while DM shares characteristics with the Ammon's horn, the V-shaped region could correspond to the DG (Atoji & Wild, 2004; Atoji et al., 2016; Herold et al., 2014). This comparison is based on the regions of intrinsic and extrinsic connectivity, as well as the receptor architecture of these areas (Atoji & Wild, 2004; Atoji et al., 2016; Herold et al., 2014). In the mammalian DG, granule cells project to CA3 via mossy fibers, but do not project outside the HF. In contrast, pyramidal cells in Ammon's horn project to regions outside of the HF such as to the septum (Spruston, 2008; Swanson & Cowan, 1977). In the avian HF, DM projects to the lateral septum and this projection is mainly glutamatergic, comparable to the projection neurons of the Ammon's horn (Atoji et al., 2016). In contrast, projections in birds arising from the V-shaped area are rather intrinsic to the HF and only very few neurons project to the septum (Atoji & Wild, 2004, 2006). Although we did not discuss the septum in our tracing experiments described above, we did observe a projection from DMd to the septum in our anterograde in vitro tracings. Moreover, in vitro injections into Vl as well as in vivo tracings that predominantly targeted the V-shaped area did not result in anterograde labeling within the septum, but rather in other hippocampal subdivisions. This confirms that projections arising from the Vl are intrinsic to the HF.

Because of their intrinsic connectivity, the V-shaped layers have already previously been compared to the mammalian DG (Atoji &

10969861, 2023, 7, Downloaded from https://onlinelibrary.wiley.com/doi/10.1002/cne.25462 by Cochrane Germany, Wiley Online Library on [28/04/2023]. See the Terms and Conditions (https://onlinelibrary.wiley.com/terms-and-conditions) on Wiley Online Library for rules of use; OA articles are governed by the applicable Creative Commons License

Wild, 2004, 2005; Atoji et al., 2016). To further investigate a possible similarity, and by inference potential homology, we looked at adult neurogenesis, a prominent feature of the mammalian DG. Neurogenesis has also already been described in several bird species including pigeons (Herold et al., 2019; Melleu et al., 2013), and can be investigated using stainings against DCX (Balthazart & Ball, 2014; Kremer et al., 2013). Our qualitative analysis of DCX expression revealed that the expression was strongest in the ventral areas such as DMvv and Vl and that the dorsomedial regions including DMvd, DMd, and Vm displayed hardly any DCX. This is in line with previous studies that quantified DCX in the avian HF and found the expression to be strongest in Vl followed by DLv and DLd, while the expression was weakest in DMd and Vm (Herold et al., 2019; Melleu et al., 2013). Similar to the DCX expression, we found GFAP-positive radial fibers mainly in DMvv and Vl. The overlapping occurrence of DCX expression and radial glia is in line with the knowledge that radial glia, in guiding neuronal migration, is involved in adult neurogenesis (Mori et al., 2005; Zupanc & Clint, 2003). These results suggest similarities of Vl and the DG, as in mammals DCX expression is strongest in DG. It is noteworthy that DCX expression in the avian brain can also be found outside of the HF (Melleu et al., 2013), which is regarded as a difference between avian and mammalian brains (Herold et al., 2014; Melleu et al., 2013). The extent of this difference, however, needs further investigation as adult neurogenesis in mammals has also been documented for other brain structures including the hypothalamus, striatum, substantia nigra, and amygdala (Jurkowski et al., 2020). Although the presence of adult neurogenesis has been established in avian HF (Barnea & Pravosudov, 2011; Hall et al., 2014; Herold et al., 2019; Hoshooley et al., 2007; Meskenaite et al., 2016; Nikolakopoulou et al., 2006), we did not further characterize the DCX-positive neurons in our study and thus cannot exclude the possibility that they represent DCX-positive neurons that were not recently generated (Bonfanti & Nacher, 2012; La Rosa et al., 2020; Luzzati et al., 2009).

Similar to DCX expression, we found that CaMKIIα expression was strongest in DMvv and Vl, although it was generally seen throughout the whole HF, albeit to a lesser extent. The CaMKIIα staining could clearly differentiate between the V-shaped layers as Vl expressed more CaMKIIα than Vm. In the mammalian HC, CaMKIIα expression is generally strong and heterogeneous but highest levels can be found within DG (Wang et al., 2013). Functionally, CaMKIIα is involved in LTP induction and in the efficiency of synaptic transmission (Wang et al., 2013). Moreover, the depletion of CaMKIIα interferes with the integration of adult-born granule cells into the circuitry of the DG (Arruda-Carvalho et al., 2014). Thus, also our CaMKIIα data underline the distinction of Vl and Vm and provide support for the similarity of Vl, rather than Vm, to DG. This comparison has also been drawn by other studies based on mRNA expression and receptor density profiles (Atoji et al., 2016; Herold et al., 2014).

For the CDL and DL, the picture is less clear as both have already been compared to the EC (Atoji & Wild, 2004, 2006; Abellán et al., 2014; Atoji et al., 2016; Herold et al., 2014, 2015). However, more detailed studies on CDL connectivity, which did not only investigate its connectivity to HF but also connections with other structures, came to the conclusion that CDL might be more similar to the cingulate cortex (Atoji & Wild, 2005). Considering these findings and the results from a receptor density study (Herold et al., 2014), we consider it more likely that the avian DL is comparable to the mammalian EC. Nevertheless, it is important to note that these subdivision-to-subdivision comparisons are confounded by the limited and mainly anatomical data in birds. More neurophysiological and functional studies of avian HF subdivisional contributions are needed. By employing newer methods and techniques that are now also available for birds, such as optogenetics (Roberts et al., 2012; Rook et al., 2021), fMRI in actively behaving animals (Behroozi et al., 2020), calcium imaging (Roberts et al., 2017), and wireless electrophysiology (Agarwal et al., 2021), the functional and neurophysiological properties of the avian HF can be further disentangled.

In summary, our study investigated the intrinsic connectivity of the avian HF at a higher spatial resolution than previous studies. We discovered a large number of previously undescribed intrahippocampal subdivisional connections as well as anatomically dissociable dorsomedial/ventrolateral processing streams along the transverse axis of the avian HF. This latter finding is consistent with reported dorsomedial/ventrolateral neurophysiological and functional differences in tufted titmice (Payne et al., 2021). We hope that our study will motivate future research, which will offer a more detailed understanding of the neurophysiological and behavioral functional contributions of the different HF anatomical subdivisions.

AUTHOR CONTRIBUTIONS

Conceptualization: Noemi Rook, Martin Stacho, Verner P. Bingman, and Onur Güntürkün. *Tracings*: Noemi Rook and Martin Stacho. *Histology*: Noemi Rook, Martin Stacho, and Ariane Schwarz. *Microscopy and data analysis*: Noemi Rook and Martin Stacho. *Original draft preparation*: Noemi Rook and Martin Stacho. *Editing*: Noemi Rook, Martin Stacho, Verner P. Bingman, and Onur Güntürkün. *Review of the final paper*: Noemi Rook, Martin Stacho, Verner P. Bingman, and Onur Güntürkün.

ACKNOWLEDGMENTS

This work was funded by the Deutsche Forschungsgemeinschaft (DFG) through SFB1372, Neu06 with project number 395940726; SFB1280, A01 with project number 316803389; and AVIAN MIND, ERC–2020–ADG, LS5, GA No. 101021354 to O.G. During a portion of this work, V.P.B. was supported by a visiting research fellowship from the Alexander Humboldt Foundation.

Open access funding enabled and organized by Projekt DEAL.

CONFLICT OF INTEREST STATEMENT

The authors declare no conflicts of interest.

DATA AVAILABILITY STATEMENT

The data that support the findings of this study are available from the corresponding author upon reasonable request.

ORCID

Noemi Rook https://orcid.org/0000-0002-2415-2813

10969861, 2023, 7, Downloaded from https://onlinelibrary.wiley.com/doi/10.1002/cne.25462 by Cochrane Germany, Wiley Online Library on [28/04/2023]. See the Terms and Conditions (https://onlinelibrary.wiley.com/terms-and-conditions) on Wiley Online Library for rules of use; OA articles are governed by the applicable Creative Commons License

PEER REVIEW

The peer review history for this article is available at https://publons.com/publon/10.1002/cne.25462.

REFERENCES

Abellán, A., Desfilis, E., & Medina, L. (2014). Combinatorial expression of Lef1, Lhx2, Lhx5, Lhx9, Lmo3, Lmo4, and Prox1 helps to identify comparable subdivisions in the developing hippocampal formation of mouse and chicken. *Frontiers in Neuroanatomy*, *8*, 59. https://doi.org/10.3389/fnana.2014.00059

Adamsky, A., Kol, A., Kreisel, T., Doron, A., Ozeri-Engelhard, N., Melcer, T., Refaeli, R., Horn, H., Regev, L., Groysman, M., London, M., & Goshen, I. (2018). Astrocytic Activation generates De Novo neuronal potentiation and memory enhancement. *Cell*, *174*, 59.e14–71.e14. https://doi.org/10.1016/j.cell.2018.05.002

Agarwal, A., Sarel, A., Derdikman, D., Ulanovsky, N., & Gutfreund, Y. (2023). Spatial coding in the hippocampus and hyperpallium of flying owls. *Proceedings of the National Academy of Sciences*, *120*(5), e2212418120. , https://doi.org/10.1073/pnas.2212418120

Amaral, D. G., & Witter, M. P. (1989). The three-dimensional organization of the hippocampal formation: A review of anatomical data. *Neuroscience*, *31*, 571–591. https://doi.org/10.1016/0306-4522(89)90424-7

Amaral, D. G., & Witter, M. P. (1995). Hippocampal formation. In G. Paxinos (Ed.), *The rat nervous system* (pp. 443–493). Academic Press.

Apostel, A., & Rose, J. (2021). Avian navigation: Head direction cells in the quail hippocampus. *Current Biology*, *31*, R781–R783. https://doi.org/10.1016/j.cub.2021.04.071

Arruda-Carvalho, M., Restivo, L., Guskjolen, A., Epp, J. R., Elgersma, Y., Josselyn, S. A., & Frankland, P. W. (2014). Conditional deletion of α-CaMKII impairs integration of adult-generated granule cells into dentate gyrus circuits and hippocampus-dependent learning. *The Journal of Neuroscience: The Official Journal of the Society for Neuroscience*, *34*, 11919–11928. https://doi.org/10.1523/JNEUROSCI.0652-14.2014

Atoji, Y., Sarkar, S., & Wild, J. M. (2016). Proposed homology of the dorsomedial subdivision and V-shaped layer of the avian hippocampus to Ammon's horn and dentate gyrus, respectively. *Hippocampus*, *26*, 1608–1617. https://doi.org/10.1002/hipo.22660

Atoji, Y., & Wild, J. M. (2004). Fiber connections of the hippocampal formation and septum and subdivisions of the hippocampal formation in the pigeon as revealed by tract tracing and kainic acid lesions. *Journal of Comparative Neurology*, *475*, 426–461. https://doi.org/10.1002/cne.20186

Atoji, Y., & Wild, J. M. (2005). Afferent and efferent connections of the dorsolateral corticoid area and a comparison with connections of the temporo-parieto-occipital area in the pigeon (*Columba livia*). *Journal of Comparative Neurology*, *485*, 165–182. https://doi.org/10.1002/cne.20490

Atoji, Y., & Wild, J. M. (2006). Anatomy of the avian hippocampal formation. *Reviews in the Neurosciences*, *17*, 3–15. https://doi.org/10.1515/REVNEURO.2006.17.1-2.3

Atoji, Y., Wild, J. M., Yamamoto, Y., & Suzuki, Y. (2002). Intratelencephalic connections of the hippocampus in pigeons (*Columba livia*). *Journal of Comparative Neurology*, *447*, 177–199. https://doi.org/10.1002/cne.10239

Bailey, D. J., Rosebush, J. C., & Wade, J. (2002). The hippocampus and caudomedial neostriatum show selective responsiveness to conspecific song in the female zebra finch. *Journal of Neurobiology*, *52*, 43–51. https://doi.org/10.1002/neu.10070

Balthazart, J., & Ball, G. F. (2014). Doublecortin is a highly valuable endogenous marker of adult neurogenesis in canaries. Commentary on Vellema M et al. (2014): Evaluating the predictive value of doublecortin as a marker for adult neurogenesis in canaries (*Serinus canaria*). J Comparative Neurol, 522:1299-1315. *Brain, Behavior and Evolution*, *84*, 1–4. https://doi.org/10.1159/000362917

Barnea, A., & Pravosudov, V. (2011). Birds as a model to study adult neurogenesis: Bridging evolutionary, comparative and neuroethological approaches. *European Journal of Neuroscience*, *34*, 884–907. https://doi.org/10.1111/j.1460-9568.2011.07851.x

Behroozi, M., Helluy, X., Ströckens, F., Gao, M., Pusch, R., Tabrik, S., Tegenthoff, M., Otto, T., Axmacher, N., Kumsta, R., Moser, D., Genc, & E., Güntürkün, O. (2020). Event-related functional MRI of awake behaving pigeons at 7T. *Nature Communications*, *11*, 4715. https://doi.org/10.1038/s41467-020-18437-1

Behroozi, M., Ströckens, F., Helluy, X., Stacho, M., & Güntürkün, O. (2017). Functional connectivity pattern of the internal hippocampal network in awake pigeons: A resting-state fMRI study. *Brain, Behavior and Evolution*, *90*, 62–72. https://doi.org/10.1159/000475591

Ben-Yishay, E., Krivoruchko, K., Ron, S., Ulanovsky, N., Derdikman, D., & Gutfreund, Y. (2021). Directional tuning in the hippocampal formation of birds. *Current Biology*, *31*, 2592.e4–2602.e4. https://doi.org/10.1016/j.cub.2021.04.029

Bonfanti, L., & Nacher, J. (2012). New scenarios for neuronal structural plasticity in non-neurogenic brain parenchyma: The case of cortical layer II immature neurons. *Progress in Neurobiology*, *98*, 1–15. https://doi.org/10.1016/j.pneurobio.2012.05.002

Broadbent, N. J., Squire, L. R., & Clark, R. E. (2004). Spatial memory, recognition memory, and the hippocampus. *Proceedings of the National Academy of Sciences of the United States of America*, *101*, 14515–14520. https://doi.org/10.1073/pnas.0406344101

Buzsáki, G. (2015). Hippocampal sharp wave-ripple: A cognitive biomarker for episodic memory and planning. *Hippocampus*, *25*, 1073–1188. https://doi.org/10.1002/hipo.22488

Canto, C. B., Wouterlood, F. G., & Witter, M. P. (2008). What does the anatomical organization of the entorhinal cortex tell us? *Neural Plasticity*, *2008*, 381243. https://doi.org/10.1155/2008/381243

Casini, G., Bingman, V. P., & Bagnoli, P. (1986). Connections of the pigeon dorsomedial forebrain studied with WGA-HRP and 3H-proline. *The Journal of Comparative Neurology*, *245*, 454–470. https://doi.org/10.1002/cne.902450403

Casper, K. B., & McCarthy, K. D. (2006). GFAP-positive progenitor cells produce neurons and oligodendrocytes throughout the CNS. *Molecular and Cellular Neurosciences*, *31*, 676–684. https://doi.org/10.1016/j.mcn.2005.12.006

Clayton, N. S., & Dickinson, A. (1998). Episodic-like memory during cache recovery by scrub jays. *Nature*, *395*, 272–274. https://doi.org/10.1038/26216

Curreli, S., Bonato, J., Romanzi, S., Panzeri, S., & Fellin, T. (2022). Complementary encoding of spatial information in hippocampal astrocytes. *PLoS biology*, *20*(3), e3001530. https://doi.org/10.1371/journal.pbio.3001530

Doron, A., Rubin, A., Benmelech-Chovav, A., Benaim, N., Carmi, T., Refaeli, R., Novick, N., Kreisel, T., Ziv, Y., & Goshen, I. (2022). Hippocampal astrocytes encode reward location. *Nature*, *609*, 772–778. https://doi.org/10.1038/s41586-022-05146-6

Erichsen, J. T., Bingman, V. P., & Krebs, J. R. (1991). The distribution of neuropeptides in the dorsomedial telencephalon of the pigeon (*Columba livia*): A basis for regional subdivisions. *Journal of Comparative Neurology*, *314*, 478–492. https://doi.org/10.1002/cne.903140306

Fujita, T., Aoki, N., Mori, C., Fujita, E., Matsushima, T., Homma, K. J., & Yamaguchi, S. (2022). Chick hippocampal formation displays subdivision- and layer-selective expression patterns of serotonin receptor subfamily genes. *Frontiers in Physiology*, *13*, 882633. https://doi.org/10.3389/fphys.2022.882633

Gagliardo, A., Ioalé, P., & Bingman, V. P. (1999). Homing in pigeons: The role of the hippocampal formation in the representation of landmarks used for navigation. *Journal of Neuroscience*, *19*, 311–315. https://doi.org/10.1523/JNEUROSCI.19-01-00311.1999

10969861, 2023, 7, Downloaded from https://onlinelibrary.wiley.com/doi/10.1002/cne.25462 by Cochrane Germany, Wiley Online Library on [28/04/2023]. See the Terms and Conditions (https://onlinelibrary.wiley.com/terms-and-conditions) on Wiley Online Library for rules of use; OA articles are governed by the applicable Creative Commons License

Gagliardo, A., Pollonara, E., Coppola, V. J., Santos, C. D., Wikelski, M., & Bingman, V. P. (2014). Evidence for perceptual neglect of environmental features in hippocampal-lesioned pigeons during homing. *European Journal of Neuroscience*, *40*, 3102–3110. https://doi.org/10.1111/ejn.12680

Garamszegi, L. Z., & Eens, M. (2004). The evolution of hippocampus volume and brain size in relation to food hoarding in birds. *Ecology Letters*, *7*, 1216–1224. https://doi.org/10.1111/j.1461-0248.2004.00685.x

Garamszegi, L. Z., & Lucas, J. R. (2005). Continental variation in relative hippocampal volume in birds: The phylogenetic extent of the effect and the potential role of winter temperatures. *Biology Letters*, *1*, 330–333. https://doi.org/10.1098/rsbl.2005.0328

Garcia, A. D. R., Doan, N. B., Imura, T., Bush, T. G., & Sofroniew, M. V. (2004). GFAP-expressing progenitors are the principal source of constitutive neurogenesis in adult mouse forebrain. *Nature Neuroscience*, *7*, 1233–1241. https://doi.org/10.1038/nn1340

Geva-Sagiv, M., Las, L., Yovel, Y., & Ulanovsky, N. (2015). Spatial cognition in bats and rats: From sensory acquisition to multiscale maps and navigation. *Nature Reviews. Neuroscience*, *16*, 94–108. https://doi.org/10.1038/nrn3888

Gupta, S., Maurya, R., Saxena, M., & Sen, J. (2012). Defining structural homology between the mammalian and avian hippocampus through conserved gene expression patterns observed in the chick embryo. *Developmental Biology*, *366*, 125–141. https://doi.org/10.1016/j.ydbio.2012.03.027

Hall, Z. J., Delaney, S., & Sherry, D. F. (2014). Inhibition of cell proliferation in black-capped chickadees suggests a role for neurogenesis in spatial learning. *Developmental Neurobiology*, *74*, 1002–1010. https://doi.org/10.1002/dneu.22180

Hartley, T., Lever, C., Burgess, N., & O'Keefe, J. (2014). Space in the brain: How the hippocampal formation supports spatial cognition. *Philosophical Transactions of the Royal Society B: Biological Sciences*, *369*, 20120510. https://doi.org/10.1098/rstb.2012.0510

Herold, C., Bingman, V. P., Strockens, F., Letzner, S., Sauvage, M., Palomero-Gallagher, N., Zilles, K., & Gunturkun, O. (2014). Distribution of neurotransmitter receptors and zinc in the pigeon (*Columba livia*) hippocampal formation: A basis for further comparison with the mammalian hippocampus. *Journal of Comparative Neurology*, *522*, 2553–2575. https://doi.org/10.1002/cne.23549

Herold, C., Coppola, V. J., & Bingman, V. P. (2015). The maturation of research into the avian hippocampal formation: Recent discoveries from one of the nature's foremost navigators. *Hippocampus*, *25*, 1193–1211. https://doi.org/10.1002/hipo.22463

Herold, C., Schlömer, P., Mafoppa-Fomat, I., Mehlhorn, J., Amunts, K., & Axer, M. (2019). The hippocampus of birds in a view of evolutionary connectomics. Cortex; a journal devoted to the study of the nervous system and behavior. *Cortex*, *118*, 165–187. https://doi.org/10.1016/j.cortex.2018.09.025

Hoshooley, J. S., Phillmore, L. S., Sherry, D. F., & MacDougall-Shackleton, S. A. (2007). Annual cycle of the black-capped chickadee: Seasonality of food-storing and the hippocampus. *Brain, Behavior and Evolution*, *69*, 161–168. https://doi.org/10.1159/000096984

Hough, G. E., & Bingman, V. P. (2004). Spatial response properties of homing pigeon hippocampal neurons: Correlations with goal locations, movement between goals, and environmental context in a radial-arm arena. *Journal of Comparative Physiology. A, Neuroethology, Sensory, Neural, and Behavioral Physiology*, *190*, 1047–1062. https://doi.org/10.1007/s00359-004-0562-z

Hough, G. E., Pang, K. C. H., & Bingman, V. P. (2002). Intrahippocampal connections in the pigeon (*Columba livia*) as revealed by stimulation evoked field potentials. *Journal of Comparative Neurology*, *452*, 297–309. https://doi.org/10.1002/cne.10409

Jurkowski, M. P., Bettio, L., K Woo, E., Patten, A., Yau, S.-Y., & Gil-Mohapel, J. (2020). Beyond the hippocampus and the SVZ: Adult neurogenesis throughout the brain. *Frontiers in Cellular Neuroscience*, *14*, 576444. https://doi.org/10.3389/fncel.2020.576444

Kahn, M. C., Hough, G. E., 2nd, Ten Eyck, G. R., & Bingman, V. P. (2003). Internal connectivity of the homing pigeon (*Columba livia*) hippocampal formation: An anterograde and retrograde tracer study. *Journal of Comparative Neurology*, *459*, 127–141. https://doi.org/10.1002/cne.10601

Kahn, M. C., Siegel, J. J., Jechura, T. J., & Bingman, V. P. (2008). Response properties of avian hippocampal formation cells in an environment with unstable goal locations. *Behavioural Brain Research*, *191*, 153–163. https://doi.org/10.1016/j.bbr.2008.03.023

Karten, H. J., & Hodos, W. (1967). A stereotaxic atlas of the brain of the pigeon (Columba Livia) (Vol. 696). Baltimore: Johns Hopkins Press.

Kerr, K. M., Agster, K. L., Furtak, S. C., & Burwell, R. D. (2007). Functional neuroanatomy of the parahippocampal region: The lateral and medial entorhinal areas. *Hippocampus*, *17*, 697–708. https://doi.org/10.1002/hipo.20315

Köbbert, C., Apps, R., Bechmann, I., Lanciego, J. L., Mey, J., & Thanos, S. (2000). Current concepts in neuroanatomical tracing. *Progress in Neurobiology*, *62*, 327–351. https://doi.org/10.1016/S0301-0082(00)00019-8

Kol, A., Adamsky, A., Groysman, M., Kreisel, T., London, M., & Goshen, I. (2020). Astrocytes contribute to remote memory formation by modulating hippocampal-cortical communication during learning. *Nature Neuroscience*, *23*, 1229–1239. https://doi.org/10.1038/s41593-020-0679-6

Krebs, J. R., Erichsen, J. T., & Bingman, V. P. (1991). The distribution of neurotransmitters and neurotransmitter-related enzymes in the dorsomedial telencephalon of the pigeon (*Columba livia*). *Journal of Comparative Neurology*, *314*, 467–477. https://doi.org/10.1002/cne.903140305

Kremer, T., Jagasia, R., Herrmann, A., Matile, H., Borroni, E., Francis, F., Kuhn, H. G., & Czech, C. (2013). Analysis of adult neurogenesis: Evidence for a prominent "non-neurogenic" DCX-protein pool in rodent brain. *PLoS ONE*, *8*, e59269. https://doi.org/10.1371/journal.pone.0059269

La Rosa, C., Parolisi, R., & Bonfanti, L. (2020). Brain structural plasticity: From adult neurogenesis to immature neurons. *Frontiers in Neuroscience*, *14*, 75. https://doi.org/10.3389/fnins.2020.00075

Lucas, J. R., Brodin, A., de Kort, S. R., & Clayton, N. S. (2004). Does hippocampal size correlate with the degree of caching specialization? *Proceedings. Biological Sciences*, *271*, 2423–2429. https://doi.org/10.1098/rspb.2004.2912

Luzzati, F., Bonfanti, L., Fasolo, A., & Peretto, P. (2009). DCX and PSA-NCAM expression identifies a population of neurons preferentially distributed in associative areas of different pallial derivatives and vertebrate species. *Cerebral Cortex*, *19*, 1028–1041. https://doi.org/10.1093/cercor/bhn145

Martinez-Gonzalez, D., Lesku, J. A., & Rattenborg, N. C. (2008). Increased EEG spectral power density during sleep following short-term sleep deprivation in pigeons (*Columba livia*): Evidence for avian sleep homeostasis. *Journal of Sleep Research*, *17*, 140–153. https://doi.org/10.1111/j.1365-2869.2008.00636.x

Mayer, U., & Bischof, H.-J. (2012). Brain activation pattern depends on the strategy chosen by zebra finches to solve an orientation task. *The Journal of Experimental Biology*, *215*, 426–434. https://doi.org/10.1242/jeb.063941

Mayer, U., Watanabe, S., & Bischof, H.-J. (2010). Hippocampal activation of immediate early genes Zenk and c-Fos in zebra finches (*Taeniopygia guttata*) during learning and recall of a spatial memory task. *Neurobiology of Learning and Memory*, *93*, 322–329. https://doi.org/10.1016/j.nlm.2009.11.006

Medina, L., Abellán, A., & Desfilis, E. (2017). Contribution of genoarchitecture to understanding hippocampal evolution and development. *Brain, Behavior and Evolution*, *90*, 25–40. https://doi.org/10.1159/000477558

Mehlhorn, J., Niski, N., Liu, K., Caspers, S., Amunts, K., & Herold, C. (2022). Regional patterning of adult neurogenesis in the homing pigeon's brain. *Frontiers in Psychology*, *13*, 889001. https://doi.org/10.3389/fpsyg.2022.889001

10969861, 2023, 7, Downloaded from https://onlinelibrary.wiley.com/doi/10.1002/cne.25462 by Cochrane Germany, Wiley Online Library on [28/04/2023]. See the Terms and Conditions (https://onlinelibrary.wiley.com/terms-and-conditions) on Wiley Online Library for rules of use; OA articles are governed by the applicable Creative Commons License

Melleu, F. F., Santos, T. S., Lino-de-Oliveira, C., & Marino-Neto, J. (2013). Distribution and characterization of doublecortin-expressing cells and fibers in the brain of the adult pigeon (*Columba livia*). *Journal of Chemical Neuroanatomy*, *47*, 57–70. https://doi.org/10.1016/j.jchemneu.2012.10.006

Meskenaite, V., Krackow, S., & Lipp, H.-P. (2016). Age-dependent neurogenesis and neuron numbers within the olfactory bulb and hippocampus of homing pigeons. *Frontiers in Behavioral Neuroscience*, *10*, 126. https://doi.org/10.3389/fnbeh.2016.00126

Montagnese, C. M., Krebs, J. R., & Meyer, G. (1996). The dorsomedial and dorsolateral forebrain of the zebra finch, *Taeniopygia guttata*: A Golgi study. *Cell and Tissue Research*, *283*, 263–282. https://doi.org/10.1007/s004410050537

Montagnese, C. M., Krebs, J. R., Székely, A. D., & Csillag, A. (1993). A subpopulation of large calbindin-like immunopositive neurones is present in the hippocampal formation in food-storing but not in non-storing species of bird. *Brain Research*, *614*, 291–300. https://doi.org/10.1016/0006-8993(93)91047-V

Morandi-Raikova, A., & Mayer, U. (2022). Spatial cognition and the avian hippocampus: Research in domestic chicks. *Frontiers in Psychology*, *13*, 1005726. https://doi.org/10.3389/fpsyg.2022.1005726

Mori, T., Buffo, A., & Götz, M. (2005). The novel roles of glial cells revisited: The contribution of radial glia and astrocytes to neurogenesis. *Current Topics in Developmental Biology*, *69*, 67–99. https://doi.org/10.1016/S0070-2153(05)69004-7

Moser, E. I., Kropff, E., & Moser, M.-B. (2008). Place cells, grid cells, and the brain's spatial representation system. *Annual Review of Neuroscience*, *31*, 69–89. https://doi.org/10.1146/annurev.neuro.31.061307.090723

Mouritsen, H., Heyers, D., & Güntürkün, O. (2016). The neural basis of long-distance navigation in birds. *Annual Review of Physiology*, *78*, 133–154. https://doi.org/10.1146/annurev-physiol-021115-105054

Nieuwenhuys, R., Voogd, J., & van Huijzen, C. (2007). *The human central nervous system: A synopsis and atlas*. Springer Science & Business Media.

Nikolakopoulou, A. M., Dermon, C. R., Panagis, L., Pavlidis, M., & Stewart, M. G. (2006). Passive avoidance training is correlated with decreased cell proliferation in the chick hippocampus. *The European Journal of Neuroscience*, *24*, 2631–2642. https://doi.org/10.1111/j.1460-9568.2006.05133.x

Payne, H. L., Lynch, G. F., & Aronov, D. (2021). Neural representations of space in the hippocampus of a food-caching bird. *Science*, *373*, 343–348. https://doi.org/10.1126/science.abg2009

Pravosudov, V. V., Kitaysky, A. S., & Omanska, A. (2006). The relationship between migratory behaviour, memory and the hippocampus: An intraspecific comparison. *Proceedings of the Royal Society B: Biological Sciences*, *273*, 2641–2649. https://doi.org/10.1098/rspb.2006.3624

Redies, C., Medina, L., & Puelles, L. (2001). Cadherin expression by embryonic divisions and derived gray matter structures in the telencephalon of the chicken. *Journal of Comparative Neurology*, *438*, 253–285. https://doi.org/10.1002/cne.1315

Roberts, T. F., Gobes, S. M. H., Murugan, M., Ölveczky, B. P., & Mooney, R. (2012). Motor circuits are required to encode a sensory model for imitative learning. *Nature Neuroscience*, *15*, 1454–1459. https://doi.org/10.1038/nn.3206

Roberts, T. F., Hisey, E., Tanaka, M., Kearney, M. G., Chattree, G., Yang, C. F., Shah, N. M., & Mooney, R. (2017). Identification of a motor-to-auditory pathway important for vocal learning. *Nature Neuroscience*, *20*, 978–986. https://doi.org/10.1038/nn.4563

Rook, N., Tuff, J. M., Isparta, S., Masseck, O. A., Herlitze, S., Güntürkün, O., & Pusch, R. (2021). AAV1 is the optimal viral vector for optogenetic experiments in pigeons (*Columba livia*). *Communications Biology*, *4*, 100. https://doi.org/10.1038/s42003-020-01595-9

Schlingloff, D., Káli, S., Freund, T. F., Hájos, N., & Gulyás, A. I. (2014). Mechanisms of sharp wave initiation and ripple generation. *Journal of Neuroscience*, *34*, 11385–11398. https://doi.org/10.1523/JNEUROSCI.0867-14.2014

Sherry, D. F., & Vaccarino, A. L. (1989). Hippocampus and memory for food caches in black-capped chickadees. *Behavioral Neuroscience*, *103*, 308–318. https://doi.org/10.1037/0735-7044.103.2.308

Siegel, J. J., Nitz, D., & Bingman, V. P. (2000). Hippocampal theta rhythm in awake, freely moving homing pigeons. *Hippocampus*, *10*, 627–631. https://doi.org/10.1002/1098-1063(2000)10:6(627::AID-HIPO1000)3.0.CO;2-W

Siegel, J. J., Nitz, D., & Bingman, V. P. (2002). Electrophysiological profile of avian hippocampal unit activity: A basis for regional subdivisions. *Journal of Comparative Neurology*, *445*, 256–268. https://doi.org/10.1002/cne.10167

Siegel, J. J., Nitz, D., & Bingman, V. P. (2005). Spatial-specificity of single-units in the hippocampal formation of freely moving homing pigeons. *Hippocampus*, *15*, 26–40. https://doi.org/10.1002/hipo.20025

Siegel, J. J., Nitz, D., & Bingman, V. P. (2006). Lateralized functional components of spatial cognition in the avian hippocampal formation: Evidence from single-unit recordings in freely moving homing pigeons. *Hippocampus*, *16*, 125–140. https://doi.org/10.1002/hipo.20139

Sievers, J., Hartmann, D., Pehlemann, F. W., & Berry, M. (1992). Development of astroglial cells in the proliferative matrices, the granule cell layer, and the hippocampal fissure of the hamster dentate gyrus. *Journal of Comparative Neurology*, *320*, 1–32. https://doi.org/10.1002/cne.903200102

Spruston, N. (2008). Pyramidal neurons: Dendritic structure and synaptic integration. *Nature Reviews Neuroscience*, *9*, 206–221. https://doi.org/10.1038/nrn2286

Striedter, G. F. (2016). Evolution of the hippocampus in reptiles and birds. *Journal of Comparative Neurology*, *524*, 496–517. https://doi.org/10.1002/cne.23803

Suárez, J., Dávila, J. C., Real, M. A., Guirado, S., & Medina, L. (2006). Calcium-binding proteins, neuronal nitric oxide synthase, and GABA help to distinguish different pallial areas in the developing and adult chicken. I. Hippocampal formation and hyperpallium. *Journal of Comparative Neurology*, *497*, 751–771. https://doi.org/10.1002/cne.21004

Swanson, L. W., & Cowan, W. M. (1977). An autoradiographic study of the organization of the efferent connections of the hippocampal formation in the rat. *Journal of Comparative Neurology*, *172*, 49–84. https://doi.org/10.1002/cne.901720104

Szkely, A. D., & Krebs, J. R. (1996). Efferent connectivity of the hippocampal formation of the zebra finch (*Taenopygia guttata*): An anterograde pathway tracing study using *Phaseolus vulgaris* leucoagglutinin. *Journal of Comparative Neurology*, *368*, 198–214. https://doi.org/10.1002/(SICI)1096-9861(19960429)368:2(198::AID-CNE3)3.0.CO;2-Z

Tömböl, T., Davies, D. C., Németh, A., Alpár, A., & Sebestény, T. (2000). A Golgi and a combined Golgi/GABA immunogold study of local circuit neurons in the homing pigeon hippocampus. *Anatomy and Embryology*, *201*, 181–196. https://doi.org/10.1007/s004290050017

Tömböl, T., Davies, D. C., Németh, A., Sebestény, T., & Alpár, A. (2000). A comparative Golgi study of chicken (*Gallus domesticus*) and homing pigeon (*Columba livia*) hippocampus. *Anatomy and Embryology*, *201*, 85–101. https://doi.org/10.1007/PL00008235

Valero, M., Cid, E., Averkin, R. G., Aguilar, J., Sanchez-Aguilera, A., Viney, T. J., Gomez-Dominguez, D., Bellistri, E., & de La Prida, L. M. (2015). Determinants of different deep and superficial CA1 pyramidal cell dynamics during sharp-wave ripples. *Nature Neuroscience*, *18*, 1281–1290. https://doi.org/10.1038/nn.4074

Wang, X., Zhang, C., Szábo, G., & Sun, Q.-Q. (2013). Distribution of CaMKIIα expression in the brain in vivo, studied by CaMKIIα-GFP mice. *Brain Research*, *1518*, 9–25. https://doi.org/10.1016/j.brainres.2013.04.042

10969861, 2023, 7, Downloaded from https://onlinelibrary.wiley.com/doi/10.1002/cne.25462 by Cochrane Germany, Wiley Online Library on [28/04/2023]. See the Terms and Conditions (https://onlinelibrary.wiley.com/terms-and-conditions) on Wiley Online Library for rules of use; OA articles are governed by the applicable Creative Commons License

Ylinen, A., Bragin, A., Nadasdy, Z., Jando, G., Szabo, I., Sik, A., & Buzsaki, G. (1995). Sharp wave-associated high-frequency oscillation (200 Hz) in the intact hippocampus: Network and intracellular mechanisms. *The Journal of Neuroscience*, *15*, 30–46. https://doi.org/10.1523/JNEUROSCI.15-01-00030.1995

Zupanc, G. K. H., & Clint, S. C. (2003). Potential role of radial glia in adult neurogenesis of teleost fish. *Glia*, *43*, 77–86. https://doi.org/10.1002/glia.10236

How to cite this article: Rook, N., Stacho, M., Schwarz, A., Bingman, V. P., & Güntürkün, O. (2023). Neuronal circuits within the homing pigeon hippocampal formation. *Journal of Comparative Neurology*, *531*, 790–813. https://doi.org/10.1002/cne.25462

10969861, 2023, 7, Downloaded from https://onlinelibrary.wiley.com/doi/10.1002/cne.25462 by Cochrane Germany, Wiley Online Library on [28/04/2023]. See the Terms and Conditions (https://onlinelibrary.wiley.com/terms-and-conditions) on Wiley Online Library for rules of use; OA articles are governed by the applicable Creative Commons License